이학석사 학위논문

Firn air age and snow density layers at Styx Glacier, East Antarctica

동남극 스틱스 빙하의 펀 공기 연령과 눈밀도 층

2019년 2월

서울대학교 대학원

지구환경과학부

장 영 준

Firn air age and snow density layers at Styx Glacier, East Antarctica

지도 교수 안 진 호

이 논문을 이학석사 학위논문으로 제출함
2019년 2월

서울대학교 대학원
지구환경과학부
장 영 준

장영준의 이학석사 학위논문을 인준함
2018년 12월

위 원 장 _____ (인)

부위원장 _____ (인)

위 원 _____ (인)

Abstract

Firn air age and snow density layers at Styx Glacier, East Antarctica

Youngjoon Jang
School of Earth and Environmental Sciences
The Graduate School
Seoul National University

Firn air provides plenty of old air from the near past, and can therefore be useful for understanding human impact on the recent history of the atmospheric composition. Most of the existing firn air records cover only the last several decades (typically 40 to 55 years) and are insufficient to understand the early part of anthropogenic impacts on atmosphere. In contrast, a few firn air records from inland sites, where temperatures and snow accumulation rates are very low, go back in time about a century. In this study, we report an unusually old firn air age of 89 years from Styx Glacier, near the Ross Sea coast in Antarctica. This is the first report of such an old firn air age (> 55 years) from a warm coastal site. The lock-in zone thickness of 12.4 m is larger than at other sites where snow accumulation rates and air temperature are similar. High-resolution X-ray density measurements demonstrate a high variability of the vertical snow density at Styx Glacier. The CH_4 mole fraction and total air content of the closed pores also indicate large variations in cm-scale depth intervals, indicative of layering. We hypothesize that the large density variations in the firn increase the thickness of lock-in zone and consequently increase firn air ages because the age of firn air rapidly increase with depth in the lock-in zone. Our study demonstrates that sites where weather conditions are favorable for the formation of large density variations at the lock-in zone preserve very old air within their open porosity, making them ideal places for firn air sampling.

Keyword : Firn air ages, Density, Layering, Methane

Student Number : 2016-20426

Table of Contents

List of Tables

List of Figures

1. Introduction

1.1 Firn structure and air transport in the firn

1.1.1 Firn ice and firn air

Bubbles trapped in ice cores preserve ancient air and allow direct measurements of the atmospheric composition in the past (e.g., Petit et al., 1999). However, it is difficult to obtain air samples over the past several decades from those ice cores since the more recent air has not yet been completely captured into bubbles closed off from the atmosphere. In contrast, we can obtain the recent records from the interstitial air in the porous, unconsolidated snow layer (firn) on top of glaciers and ice sheets (Etheridge et al., 1996, 1998). In addition, we can take advantage of the very large amount of firn air because it allows us to accurately analyze isotopic ratios of greenhouse gases and many trace gases such as man-made CFCs, HCFCs and SF_6 (Buizert et al., 2012a; Laube et al., 2012). However, reported firn air ages date back only several decades at the sites where snow accumulation rates are relatively high (Table 1). Old firn air (> 55 years) was observed only at sites where surface temperatures and snow accumulation rates are low such as South Pole and inland Antarctic Megadunes (Table 1); however, even under such circumstances very old firn air is not guaranteed, as demonstrated by Dome C (Table 1).

In the firn layer, air moves through the open pores and is occluded into the adjacent ice at the typical close-off density (Schwander, 1989). The firn air moves downward with the adjacent ice (advection), but is furthermore mixed by diffusion, and affected by thermal and gravitational fractionation (Craig et al., 1988; Johnsen et al., 2000; Severinghaus et al., 2001; Goujon et al., 2003). In addition,

the gradual bubble trapping in the firn affects the movement of the air. As a result, at each depth there is a gas age distribution (Trudinger et al., 1997), rather than a single gas age. Therefore, studying firn air is also important for interpreting the record of ancient air trapped in ice cores.

1.1.2 Firn air transport and zonal description

The firn column is generally divided into three zones; convective, diffusive and lock-in zones, depending on the mechanisms of firn air movement (Sowers et al., 1992). The convective zone is the upper part of the firn where the air can ventilate with the overlying atmosphere. With stronger wind pumping, there can be a deeper convective zone (Kawamura et al., 2013). This zone has the same $\delta^{15}N$ of N_2 value as that of the atmosphere. The diffusive zone is located under the convective zone, where molecular diffusion of the firn air dominates transport mechanism of the firn air (Blunier and Schwander, 2000). The age of the firn air increases slowly with depth in the diffusive zone because of continued gas exchange with atmospheric air via diffusion. Heavier isotopes are enriched with depth due to the gravitational fractionation in the stagnant diffusive layer. Thus, $\delta^{15}N$ of N_2 gradually increases with depth in the diffusive zone. In the lock-in zone (LIZ) below the diffusive zone, gas diffusion is strongly impeded although the bubbles are not entirely closed. The top of the lock-in zone is called lock-in depth (LID), where the gravitational fractionation ceases, so that the $\delta^{15}N$ of N_2 becomes constant. The bottom of the LIZ is defined as the close-off depth (COD), where all air bubbles are closed off and firn becomes mature ice. The COD can be estimated in two different ways.

First, we can calculate the COD from firn densification models. Typically, the close−off occurs the density of ice reaches about 830 kg m^{-3} (Blunier and Schwander, 2000). – equivalent to a critical porosity of around 0.1 (Schaller et al., 2017). Also, if temperature is known, the average density at close−off can be estimated from empirical relations (Martinerie et al., 1992). Second, the deepest position where air can be sampled from the firn column is commonly considered as (just above) the COD. In theory, the COD is the depth at which all pores are closed, but it can be ambiguous to specify the COD in the field because firn air can be sampled at a slightly deeper depth than that of the shallowest impermeable snow layer due to the existence of permeable layers at deeper depths – this effect is due to density layering (Mitchell et al., 2015).

The gas ages in the LIZ increase with depth faster than in the diffusive zone. In the LIZ, firn air moves downward at (nearly) the same rate as the surrounding ice, and therefore the age of the air increases with depth at the same rate as the age of ice.

1.2 Firn air age and snow density layers

1.2.1 Firn air age

The age of the firn air is directly related to the movement of the firn air. We define the oldest firn air age as the mean age at the deepest sampling depth −. The firn air models help calculate the firn air age using some parameters such as temperature and accumulation rate. However, several studies found that the layering also affects the movement of the firn air (e.g., Mitchell et al., 2015; Schaller et al., 2017). This implies that physical properties of the ice may affect the age of the firn air as well.

1.2.2 Snow density layers

With regard to the lock-in and close-off processes, recent studies have focused on snow layers and microstructure of the firn (Hörhold et al., 2011; Gregory et al., 2014; Mitchell et al., 2015; Schaller et al., 2017). Density variability on millimeter to tens of cm scales is observed in all polar sites. Hörhold et al. (2011) demonstrate that density variability is caused by physical snow properties in the firn column. Several studies have dealt with how snow density variations affect the transport of firn air (Hörhold et al., 2011; Mitchell et al., 2015). Mitchell et al. (2015) showed that the firn layering can affect the closure of pores and the thickness of LIZ, but the relation between snow density variations and range of firn air ages was not quantitatively examined.

In this study, we present firn air compositions and $\delta^{15}N-N_2$ from Styx Glacier, East Antarctica to better understand the role of snow density variations on the age of firn air. We also present X-ray density data with millimeter resolutions and compare them with $\delta^{18}O_{ice}$ and the closed-pore air compositions in the LIZ.

We hypothesize that large snow density variations make the LIZ thicker and facilitate preservation of old firn air at the Styx Glacier. This study will help us better understand how the snow density layers of firn column affects movement and preservation of firn air, and provide guidance on selecting good sites for future firn air studies.

2. Materials and Methods

2.1 Firn air sampling and gas mole fractions analysis

The firn air and ice core were sampled at the Styx Glacier, East Antarctica (73° 51.10' S, 163° 41.22' E, 1623 m asl) in December of 2014 (Fig. 1). This site is located 85 km north of the Korean Jang Bogo Station in the Southern Cross Mountains near the Ross Sea (Han et al., 2015). The snow accumulation rate is ~10 cm ice $year^{-1}$ that was calculated from the Styx16b ice chronology based on methane correlation and tephra age tie-point and thinning functions (Yang et al., 2018). The mean annual surface temperature was measured as −31.7℃ by borehole temperature logging at 15 m depth, two-year after the ice core drilling (Yang et al., 2018). Table 1 lists the characteristics of the Styx Glacier and other firn air sampling sites. A total of 13 samples from the surface to 64.8 m depth were collected. The firn air sampling device was constructed, following the design of that of the University of Bern, Switzerland (Schwander et al., 1993). Three vacuum pumps (two diaphragm pumps and one metal bellows pump), several pressure gauges, stainless steel lines, and vacuum valves were housed in an aluminum case to transfer to the polar site. The pump system plays four major roles: (1) purging modern air from the bottom of a borehole, (2) inflating the bladder to block the deep firn layers from the atmosphere, (3) removing the contaminated air and extracting the firn air, (4) transporting firn air to a CO_2 analyzer for measurements of gas mole fractions and store it in firn air containers. The bladder system is designed to be lowered into the borehole to seal the deep firn layer(s) being sampled from the atmosphere. The bladder

consists of a 4 m−long rubber tube and metal caps on top and bottom of the rubber tube. The bladder’ s external diameter is 119.5 mm and internal diameter is 114.5 mm. The material of the tube is butyl rubber (BIIR) which can endure being inflated in low temperatures.

The firn air samples were collected in 3−liter glass flasks at all collection depths. However, to test preservation ability of the sample air containers, Silcocan canisters were also used at 4 depths (0, 35.36, 43.42, 53.95 m). Accurate mole fractions of CO_2, CH_4, and SF_6 were measured at US National Oceanic and Atmospheric Administration (NOAA; https://www.esrl.noaa.gov/). The results for the two types of containers show good agreements. $\delta^{15}N$ of N_2 was analyzed at Scripps Institution of Oceanography for correcting gravitational fractionation effect (Severinghaus et al., 2010).

2.2 Firn air transport model

We used the Center for Ice and Climate (CIC) firn air model which is a 1−dimensional diffusion model to simulate how the air moves in Styx firn column. In this model, there are 4 types of transport in the open porosity: (1) molecular diffusion, (2) vigorous mixing in the convective zone, (3) advection, and (4) dispersion in the deep firn (Buizert, 2012b, Buizert and Severinghaus, 2016). A velocity of the air is represented as w_{air} in open pores.

$$w_{\mathrm{air}} = \frac{A\,\rho_{\mathrm{ice}}}{s_{\mathrm{op}}^{*} P_0}\left(\frac{s_{\mathrm{cl}}(z_{\mathrm{COD}})P_{\mathrm{cl}}(z_{\mathrm{COD}})}{\rho_{\mathrm{COD}}} - \frac{s_{\mathrm{cl}}(z)P_{\mathrm{cl}}(z)}{\rho(z)}\right) \quad (1)$$, where

A is the accumulation rate (0.10 m ice yr^{-1}), z_{COD} is the full close−off depth, ρ_{ice} is the density of ice (0.921 g cm^{-3}), s_{op}^{*} is the effective open porosity, s_{cl} is the closed porosity, and P_o and P_{cl} is the enhanced pressure due to firn compaction in closed bubbles. Other variables are expressed in Table 1.

2.3 CH_4 in closed bubbles and total air content measurements

CH_4 CH_4 mole fraction in the (closed) air bubbles in the firn ice was measured at Seoul National University by a wet extraction method which extracts air from the ice by thawing and refreezing (Yang et al., 2017). 124 discrete firn ice samples (cross section of 8.5 cm × 3 cm, length of 3 cm, ~35 g) were prepared from 4 different depth intervals in the lock-in zone (54.59-55.34, 58.11-59.05, 59.86-60.55, 64.02-65.25 m). All ice samples were cut and trimmed by ~2.5 mm with a band saw to remove the surface ice. Then, the ice samples were inserted into the glass flasks attached to the gas extraction line. The pump system evacuated air in the flask in the cooled ethanol bath at −70 ℃ for 20 min. After the pressure dropped below 0.2 mTorr, the ice samples in the glass flask were melted and air in the bubbles were extracted. After the melting was finished, we refroze the ice using a cooled ethanol bath to release the gas dissolved in the ice melt. Finally, the extracted air was injected into the sample loop of the gas chromatograph equipped with a flame ionization detector (FID). The calibration curve of the GC-FID was calculated by standard air with the CH_4 mole fraction of 895 ppbv on the NOAA04 scale (Dlugokencky et al., 2005).

2.4 Analysis for stable isotopes of ice

After the measurement of the CH_4 mole fraction in air, the melt water was put into cleaned 125 ml bottles and analyzed for water stable isotope ratios at Korea Polar Research Institute (KOPRI) using a Cavity Ring-Down Spectroscopy (CRDS, L1102-i, Picarro, USA)

system. The data are here presented as δ-notations ($\delta^{18}O(‰) = (({}^{18}O/{}^{16}O)_{sample}/({}^{18}O/{}^{16}O)_{VSMOW} - 1) \times 1000$, $\delta D(‰) = (({}^{2}H/{}^{1}H)_{sample}/({}^{2}H/{}^{1}H)_{SMOW} - 1) \times 1000)$). The firn ice melt was filled into a 400 μl insert in a 2 ml glass vial using a syringe filter. The auto sampler transported the ice melt samples in the insert to the vaporizer about 180 nL at a time. The samples with the liquid state were transferred to the cavity after being converted into the water vapor in a vaporizer at 110 ℃. The measurement precision evaluated by measuring an in-house standard repeatedly (n=12) was 0.08‰ for $\delta^{18}O$ and 0.3‰ for δD (1 sigma standard deviations).

2.5 X-ray firn density measurement

We obtained high-resolution density data using the X-ray transmission method reported by Hori et al. (1999) for the firn ice at various depth intervals. This method is advantageous because it can measure continuously and non-destructively. The X-ray beam penetrates the ice samples and the detector on the opposite side analyzes the intensity of the beam. To make equal thickness for each core section, upper and side parts of the half circle-shape core were shaved by a microtome. After putting the precut ice core on a rack, we set the rate of measurement at 50 mm min^{-1}, and finally obtained 1mm-resolution density data.

3. Results

3.1 Layered stratigraphy

We examined a snow pit, located 10 m away from the main ice core borehole, 2 years after drilling to understand the physical properties such as layers, density, and ice grain size of the upper firn at Styx site. We scratched the snow wall by hand to remove soft layers and enhance the visibility of hard layers (Fig. 2a). The soft layers have low density and are presumed to be depth hoarse, and the hard ones are wind crusts with high density (Fig. 2b). The alternating layers repeat with intervals of few centimeters to 20 centimeters. The top boundaries of the hard layers are sharp and extend horizontally about a meter, but the bottom boundaries are not well defined due to gradual density changes. 10 cm-resolution density data were obtained by a density cutter (Proksch et al., 2016). The density is low in coarse-grained layers, while it is high in fine-grained layers (Fig. 2b-d).

3.2 Firn gas sampling and the age of firn air

We calibrate the depth-diffusivity profile in the model using trace gases with a well-known atmospheric history (Buizert et al., 2012a; Trudinger 1997; Rommelaere 1997). The atmospheric time series from well-dated firn air (Etheridge et al. 1996, 1998) and instrument measurement records (NOAA; https://www.esrl.noaa.gov/) were used for calibration. The simulated mole fraction profiles match well with the observations (Fig. 3). CO_2, CH_4, SF_6 and $\delta^{15}N-N_2$ distributions in firn air were modeled. The model does not include thermal fractionation, and therefore provides a poor fit to the $\delta^{15}N-N_2$ data in the upper firn where seasonal temperature gradients fractionate the gases. The firn air age (black curves in Fig. 3) slowly

increases with depth at the diffusive zone because it mixes with fresh atmospheric air on the surface mostly by molecular diffusion (Blunier and Schwander, 2000). In contrast, the firn air age rapidly increases with the same rate of the surrounded ice age in the LIZ.

The lowest CO_2 mole fraction of 305.18 ppmv at depth of 64.8 m corresponds to the year of 1927 or mean age of 89 years (relative to sampling year 2014) on the Law Dome ice core record (MacFarling Meure et al., 2006). We also obtained the CH_4 mole fraction of 943.36 ppbv at the same depth, which corresponds to an age of 88 years (MacFarling Meure et al., 2006) (Figs. 3a, 3b). Each gas has different modeled ages because their diffusivities are different. Only few studies have reported firn air ages older than 89 years: 93 years from the South Pole (Severinghaus et al., 2001) and 121 years from Megadunes (Severinghaus et al., 2001; Fig. 4). These sites are located inland Antarctica and have low annual mean temperatures and low snow accumulation rates (Table 1). Firn densification takes a long time if snow accumulation is low, therefore the firn air can be preserved for a long time without being trapped. In contrast, Styx site is located near the coast and has relatively high snowfall, and therefore the age of 89 years is very unusual. Sites of comparable climate characteristics typically have an oldest firn air age of around 40 years. This indicates that there may be other factors that can permit preservation of the old firn air at Styx Glacier.

3.3 Density layering and its influence on bubble trapping

Firn density is the primary control on the bubble close-off process, and therefore density layering leads to staggered bubble trapping,

with high-density layers closing off before low-density ones (Etheridge et al. 1992, Mitchell et al. 2015, Rhodes et al. 2016).

Because the atmospheric CH_4 mole fraction has increased during the last century, we may obtain information on the timing of the bubble close-off from the CH_4 mole fraction of the air trapped in closed bubbles ($[CH_4]_{cl}$). In this study, we used the $[CH_4]_{cl}$ and total air content of the firn ice as indicators of the close-off process. The density and $[CH_4]_{cl}$ show an anti-correlation (Fig. 5). High-density layers reach the lock-in and close-off densities at shallower depths than low-density layers do. Thus, air bubbles are trapped at shallower depths in high-density layers. Early trapped bubbles preserve older air with lower greenhouse gas mole fractions. Meanwhile, higher air content is expected in the high-density layers, in which open porosity is small and closed porosity is large (Fig. 5). However, we cannot entirely exclude the possibility of some post-coring bubble close-off. High open porosity in low-density layers may have more chances to trap modern ice storage air, which has higher mole fraction of CH_4 than atmospheric background levels.

Figure 5a shows $[CH_4]_{cl}$ and total air contents in the LIZ of the Styx firn. $[CH_4]_{cl}$ generally decreases with depth and the variations are stabilized at a deeper layer, while the total air content generally increases with depth. The $[CH_4]_{cl}$ greater than CH_4 mole fraction in neighboring firn air (green line in Fig. 5a) indicates part of bubbles formed after coring and increased the $[CH_4]_{cl}$, as previous studies also observed (Mitchell et al., 2015; Rhodes et al., 2013). Most of $[CH_4]_{cl}$ data show large cm-scale variations (Fig. 5). The highs and lows of $[CH_4]_{cl}$ repeat with cycles of 6 cm to 24 cm (Fig. 5b). Note that the layering observed in the snow pit likewise showed irregular

intervals (Fig. 2b). From the layer spacing, we conclude that bubble trapping at Styx is not controlled by annual layers (Section 4), as was observed at Law Dome (Etheridge et al. 1992).

The evolution of CH_4 in the closed porosity may give information on how the snow layers can make inhomogenous records and how the gas age distribution is determined in ice core studies (Fourteau et al. 2017, www.clim-past.net/13/1815/2017/). However, the details are beyond the scope of this study and we will focus on the firn air age in the open porosity.

3.4 High-resolution firn density measurements

The X-ray measurements show highly variable density on cm scales. We converted the high-resolution density to total porosity using the following equation:

$$\Phi_{\text{total}} = 1 - \frac{\rho}{\rho_{\text{ice}}} \quad (3)$$

where ρ = density of porous ice; ρ_{ice} = density of bubble-free ice (919 kg m^{-3}); and Φ = porosity.

At Styx Glacier, the shallowest depth, where the running mean of total porosity with a 1 cm-thick window reaches below 0.1, is 48.1 m (Figs. 6a and 6b). It is approximately 4.3 m shallower than the LID of 52.4 m defined by the firn air $\delta^{15}N-N_2$. Meanwhile, the deepest point, where the running mean (with a 1 cm-thick window) becomes less than 0.1, is at 63.7 m (Figs. 6a and 6c), which is shallower than the COD of 64.8 m defined by the deepest successful firn pumping depth. Although the LID and COD from the density data are different from those defined by firn air data, the thickness of LIZ from density data is comparable to that from firn air analysis (between two blue

lines in Fig. 6). The offsets of the LIZ about 1–4 m between those from total porosity and the firn air measurement may be due to the fact that actual critical porosity may be variable and depend on study sites, perhaps depending on horizontal snow density variations and the horizontal extent of diffusion–impeding layers. In spite of the possibilities of error, the similarity in the LIZ thicknesses from the two methods support the idea that the large variations of density can increase the LIZ thickness by shallowing LID and/or deepening the COD. The thick LIZ eventually permits storing old firn air at Styx (Table 1). We demonstrate here that the snow density variability is an important factor in determining the firn air age. We suggest that sites with higher density variations at the LIZ have a high possibility of a thick LIZ and therefore old firn air, even in warm, high–precipitation coastal climates.

4. Discussions

To quantitatively compare density variability of Styx snow with those at other glacier sites, we may use the standard deviation of densities (σ_ρ) near the mean air–isolation density (Hörhold et al., 2011; Martinerie et al., 1992). The mean density at the mean air–isolation depth (ρ_{crit}) can be related to mean annual temperature (T in Kelvin) using the following equation, which is empirically obtained from air content measurements (Martinerie et al., 1992):

$$\rho_{crit} = \left(\frac{1}{\rho_{ice}} + 7.6 \times 10^{-4} \times T - 0.057\right)^{-1} \quad (4),$$

where ρ_{ice} is the density of bubble–free pure ice.

Although this equation cannot provide exact ρ_{crit}, we can take advantage in estimating the density at LIZ without gas chemistry data (Hörhold et al., 2011). Using the Styx high–resolution X–ray density data at depth interval of 43.13–66.97 m, we calculated the standard deviation of densities (σ_ρ). For each σ_ρ, we used 1000 density data points (Fig. 7) as Hörhold et al. (2011) did (Table 2). At Styx, ρ_{crit} is 821.68 kg m^{-3} according to equation (4), and the standard deviation of densities at ρ_{crit} (σ_ρ, ρ_{crit}) is 19.33±1.87 kg m^{-3}, which is greater than those in the other previously studied sites (Fig. 7, Table 2). The high σ_ρ, ρ_{crit} at Styx likely facilitates the thick LIZ and old firn air. A high snow accumulation rate may not allow old firn air ages for a certain LIZ thickness. Thus, σ_ρ, ρ_{crit} divided by a snow accumulation rate (A) can be a better indicator of the range of air ages. The Styx (σ_ρ, ρ_{crit} / A) is also greater than other studied sites (Table 2).

A high–density (low–density) layer at surface may become a low–density (high–density) layer (Freitag et al., 2004; Fujita et al.,

2009) at density of 600–650 kg m^{-3}, which occurs at shallower depths than LIZ (Hörhold et al., 2011). Thus, vertical snow layering at surface may not directly give information about density variability at LIZ (Hörhold et al., 2011). However, conditions for snow layering at the surface still may give us clues on the density variability at LIZ. The conditions may include redistribution of snow by wind and formation of wind and/or radiation crusts (Martinerie et al., 1992; Hörhold et al., 2011). To test the possibility of seasonal causes, we analyzed stable isotopes of surface snow ($\delta^{18}O$) because the surface $\delta^{18}O$ generally follows seasonal variation (depleted in winter and enriched in summer). Figures 2e and 2f show the stable isotope profiles of snow ($\delta^{18}O$) at Styx Glacier, which are apart by ~100 m; one is from a snow pit made in 2014 and the other is from the main ice core drilled in 2014. The $\delta^{18}O$ profiles commonly show cycles with intervals of ~40 cm per year, given that local maxima of $\delta^{18}O$ indicate summer, and minima winter layers. Meanwhile, the repetition of the density layers has twenty cycles (high and low density layer pairs) in the top 180 cm depth at the snow pit (Fig. 2b). Applying the snow accumulation rate of ~40 cm y^{-1} in recent years, the density layers have 4~5 cycles y^{-1}, indicating that the formation of snow density layers is mainly controlled by non–seasonal factors.

A blizzard occurred during the ice coring campaign in December of 2014. We observed that the blizzard strongly reworked the surface snow. The Automatic Weather System (AWS) installed within 10 m from the borehole site show that blizzard events (wind speed > 15 m s^{-1}) took place on December 29 in 2015, May 23, June 26, August 17, and September 7 in 2016 (Fig. 8). The number of blizzard events in a year is similar to the mean density layer cycle of 4~5 y^{-1}. Although Blizzard occurs more frequently in winter, the frequency of

5 yr^{-1} is comparable to the number of the density layer cycles of 4~5 yr^{-1}. At the time intervals, westerly wind prevailed. When redeposited by a blizzard event, particles of snow can be sorted (Sepp Kipfstuhl, personal communications) and following solar radiation and temperature gradient may facilitate diagenesis of the snow layers (Alley, 1988; Fegyveresi et al., 2018). During the diagenesis processes, fine and coarse flake layers may form high-density and low-density layers, respectively.

5. Conclusions and implications

About 89-year-old firn air was found at Styx Glacier, East Antarctica, located near the Ross Sea coast. This is of great scientific interest because such old firn air is commonly only found in the inland sites such as the South Pole and Megadunes. The thickness of Styx LIZ is relatively greater than those in other sites where snow accumulation and temperature are similar. The thicker LIZ made the Styx firn layer preserve old firn air because the age of stagnant firn air rapidly increases with depth in the LIZ as air exchange with the atmosphere has stopped. We hypothesized that the high snow density variations at the LIZ of Styx Glacier made the thick LIZ and old firn air. To test the hypothesis, we conducted high-resolution X-ray density measurements. We argue that the thick LIZ is related to the high density variations at Styx Glacier. We also examined why high snow density variability developed at Styx site. The effect of strong wind (e.g., blizzards) may facilitate the density layer formation. It is likely that old firn air (>55 years) can be found in areas where climatological conditions are favorable for high snow density variations at LIZ even when the sites are located near the coast. We may take advantage in sampling and transportation from the coastal sites, because logistics is easier for those sites.

References

Alley, R. B.: Concerning the Deposition and Diagenesis of Strata in Polar Firn, Journal of Glaciology, 34, 283–290, http://dx.doi.org/10.3189/s0022143000007024, 1988.

Battle, M. O., Severinghaus, J. P., Sofen, E. D., Plotkin, D., Orsi, A. J., Aydin, M., Montzka, S. A., Sowers, T., and Tans, P. P.: Controls on the movement and composition of firn air at the West Antarctic Ice Sheet Divide, Atmospheric Chemistry and Physics Discussions, 11, 18633–18675, http://dx.doi.org/10.5194/acpd-11-18633-2011, 2011.

Blunier, T. and Schwander, J.: Gas enclosure in ice: age difference and fractionation, in: Physics of Ice Core Records, edited by: Hondoh, T., Hokkaido University Press, Sapporo, 307–326, 2000.

Buizert, C., Martinerie, P., Petrenko, V. V., Severinghaus, J. P., Trudinger, C. M., Witrant, E., Rosen, J. L., Orsi, A. J., Rubino, M., Etheridge, D. M., Steele, L. P., Hogan, C., Laube, J. C., Sturges, W. T., Levchenko, V. A., Smith, A. M., Levin, I., Conway, T. J., Dlugokencky, E. J., Lang, P. M., Kawamura, K., Jenk, T. M., White, J.W. C., Sowers, T., Schwander, J., and Blunier, T.: Gas transport in firn: multiple-tracer characterisation and model intercomparison for NEEM, Northern Greenland, Atmos. Chem. Phys., 12, 4259–4277, doi:10.5194/acp-12-4259-2012, 2012a.

Buizert, C.: The influence of firn air transport processes and radiocarbon production on gas records from polar firn and ice, PhD, Faculty of Science, University of Copenhagen, Denmark, Copenhagen, 175 pp., 2012b.

Buizert, C. and Severinghaus, J. P.: Dispersion in deep polar firn driven by synoptic-scale surface pressure variability, The Cryosphere, 10, 2099–2111, https://doi.org/10.5194/tc-10-

2099–2016, 2016.

Craig, H., Horibe, Y., and T., S.: Gravitational separation of gases and isotopes in polar ice caps, Science, 242, 1675–1678, 1988.

Dlugokencky, E. J., Myers, R. C., Lang, P. M., Masarie, K. A., Crotwell, A. M., Thoning, K. W., Hall, B. D., Elkins, J. W., and Steele, L. P.: Conversion of NOAA atmospheric dry air CH4 mole fractions to a gravimetrically prepared standard scale, J. Geophys. Res., 110, D18306, https://doi.org/10.1029/2005JD006035, 2005.

Etheridge, D. M., Pearman, G. I., and Fraser, P. J.: Changes in tropospheric methane between 1841 and 1978 from a high accumulation–rate Antarctic ice core, Tellus B, 44, 282–294, doi:10.1034/j.1600–0889.1992.t01–3–00006.x, 1992.

Etheridge, D. M., Steele, L. P., Langenfelds, R. L., Francey, R. J., Barnola, J. M., and Morgan, V. I.: Natural and anthropogenic changes in atmospheric CO2 over the last 1000 years from air in Antarctic ice and firn, J. Geophys. Res., 101, 4115–4128, doi:10.1029/95jd03410, 1996.

Etheridge, D. M., Steele, L. P., Francey, R. J. and Langenfelds, R. L.: Atmospheric methane between 1000 A.D. and present: Evidence of anthropogenic emissions and climatic variability, Journal of Geophysical Research, 103(D13), 15979, doi:10.1029/98JD00923, 1998.

Fegyveresi, J. M., Alley, R. B., Muto, A., Orsi, A. J., and Spencer, M. K.: Surface formation, preservation, and history of low–porosity crusts at the WAIS Divide site, West Antarctica, The Cryosphere, 12, 325–341, http://dx.doi.org/10.5194/tc–12–325–2018, 2018.

Freitag, J., Wilhelms, F., and Kipfstuhl, S.: Microstructure dependent densification of polar firn derived from X–ray microtomography, J. Glaciol., 50, 243–250, 2004.

Fujita, S., Okuyama, J., Hori, A., and Hondoh, T.: Metamorphism of stratified firn at dome fuji, antarctica: A mechanism for local insolation modulation of gas transport conditions during bubble close off, J. Geophys. Res., 114, F03023, doi:10.1029/2008JF001143, 2009.

Goujon, C., Barnola, J. M., and Ritz, C.: Modeling the densification of polar firn including heat diffusion: Application to closeoff characteristics and gas isotopic fractionation for Antarctica and Greenland sites, J. Geophys. Res.-Atmos, 108, 4792, doi:10.1029/2002JD003319, 2003.

Gregory, S. A., Albert, M. R., and Baker, I.: Impact of physical properties and accumulation rate on pore close-off in layered firn, The Cryosphere, 8, 91-105, http://dx.doi.org/10.5194/tc-8-91-2014, 2014.

Han, Y., Jun, S. J., Miyahara, M., Lee, H.-G., Ahn, J., Chung, J. W., Hur, S. D., and Hong, S. B.: Shallow ice-core drilling on Styx glacier, northern Victoria Land, Antarctica in the 2014-2015 summer, Journal of the Geological Society of Korea, 51, 343-355, 2015

Hörhold, M. W., Kipfstuhl, S., Wilhelms, F., Freitag, J., and Frenzel, A.: The densification of layered polar firn, Journal of Geophysical Research: Earth Surface, 116, http://dx.doi.org/10.1029/2009jf001630, 2011.

Hori, A., Tayuki, K., Narita, H., Hondoh, T., Fujita, S., Kameda, T., Shoji, H., Azuma, N., Kamiyama, K., Fujii, Y., Motoyama, H., and Watanabe, O.: A detailed density profile of the Dome Fuji (Antarctica) shallow ice core by X-ray transmission method, Annals of Glaciology, 29, 211-214, http://dx.doi.org/10.3189/172756499781821157, 1999.

Johnsen, S. J., Clausen, H. B., Cuffey, K. M., Hoffmann, G., Schwander, J., and Creyts, T.: Diffusion of stable isotopes in polar firn and ice: the isotope effect in firn diffusion, in: Physics of Ice Core Records, edited by: Hondoh, T., vol. 159, 121–140, Hokkaido University Press, Sapporo, Japan, 2000.

Kawamura, K., Severinghaus, J. P., Albert, M. R., Courville, Z. R., Fahnestock, M. A., Scambos, T., Shields, E., and Shuman, C. A.: Kinetic fractionation of gases by deep air convection in polar firn, Atmospheric Chemistry and Physics, 13, 11141–11155, http://dx.doi.org/10.5194/acp-13-11141-2013, 2013.

Landais, A., Barnola, J.M., Kawamura, K., Caillon, N., Delmotte, M., Van Ommen, T., Dreyfus, G., Jouzel, J., Masson-Delmotte, V., Minster, B., Freitag, J., Leuenberger, M., Schwander, J., Huber, C., Etheridge, D., and Morgan, V.: Firn-air δ15N in modern polar sites and glacial–interglacial ice: a model-data mismatch during glacial periods in Antarctica?, Quaternary Science Reviews, 25, 49-62, http://dx.doi.org/10.1016/j.quascirev.2005.06.007, 2006.

Laube, J. C., Hogan, C., Newland, M. J., Mani, F. S., Fraser, P. J., Brenninkmeijer, C. A. M., Martinerie, P., Oram, D. E., Röckmann, T., Schwander, J., Witrant, E., Mills, G. P., Reeves, C. E., and Sturges, W. T.: Distributions, long term trends and emissions of four perfluorocarbons in remote parts of the atmosphere and firn air, Atmos. Chem. Phys., 12(9), 4081-4090, 2012.

MacFarling-Meure, C., Etheridge, D., Trudinger, C., Steele, P., Langenfelds, R., van Ommen, T., Smith, A., and Elkins, J.: Law Dome CO2, CH4 and N2O ice core records extended to 2000 years BP, Geophys. Res. Lett., 33, L14810, doi:10.1029/2006GL026152, 2006.

Martinerie, P., Raynaud, D., Etheridge, D. M., Barnola, J. M., and

Mazaudier, D.: Physical and Climatic Parameters which Influence the Air Content in Polar Ice, Earth Planet. Sc. Lett., 112, 1–13, doi:10.1016/0012–821X(92)90002–D, 1992.

Mitchell, L. E., Buizert, C., Brook, E. J., Breton, D. J., Fegyveresi, J., Baggenstos, D., Orsi, A., Severinghaus, J., Alley, R. B., Albert, M., Rhodes, R. H., McConnell, J. R., Sigl, M., Maselli, O., Gregory, S., and Ahn, J.: Observing and modeling the influence of layering on bubble trapping in polar firn, J. Geophys. Res.–Atmos., 120, 2558–2574, https://doi.org/10.1002/2014JD022766, 2015.

Petit, J. R., Jouzel, J., Raynnaud, D., Barkov, N. I., Barnola, J.–M., Basile, I., Bender, M., Chappellaz, J., Davis, M., Delaygue, G., Delmotte, M., Kotlyakov, V. M., Legrand, M., Lipenkov, V. Y., Lorius, C., Pepin, L., Ritz, C., Saltzman, E., and Stievenard, M.: Climate and atmospheric history of the past 420 000 years from the Vostok ice core, Antarctica, Nature, 399, 429–436, 1999.

Proksch, M., Rutter, N., Fierz, C., and Schneebeli, M.: Intercomparison of snow density measurements: bias, precision, and vertical resolution, The Cryosphere, 10, 371–384, doi:10.5194/tc–10–371–2016, 2016.

Rhodes, R. H., Fain, X., Stowasser, C., Blunier, T., Chappellaz, J., McConnell, J. R., Romanini, D., Mitchell, L. E., and Brook, E. J.: Continuous methane measurements from a late Holocene Greenland ice core: atmospheric and in–situ signals, Earth Planet. Sc. Lett., 368, 9–19, 2013.

Rhodes, R. H., Faïn, X., Brook, E. J., McConnell, J. R., Maselli, O. J., Sigl, M., Edwards, J., Buizert, C., Blunier, T., Chappellaz, J., and Freitag, J.: Local artifacts in ice core methane records caused by layered bubble trapping and in situ production: a multi–site investigation, Clim. Past, 12, 1061–1077, doi:10.5194/cp–12–

1061– 2016, 2016.

Rommelaere, V., Arnaud, L., and Barnola, J. M.: Reconstructing recent atmospheric trace gas concentrations from polar firn and bubbly ice data by inverse methods, J. Geophys. Res.–Atmos., 102, 30069–30083, doi:10.1029/97JD02653, 1997.

Schaller, C. F.., Freitag, J., and Eisen, O.: Critical porosity of gas enclosure in polar firn independent of climate, Climate of the Past, 13, 1685–1693, http://dx.doi.org/10.5194/cp–13–1685–2017, 2017.

Schwander, J.: The transformation of snow to ice and the occlusion of gases, Environ. Rec. Glaciers Ice Sheets, 8, 53–67, 1989.

Schwander, J., Barnola, J.–M., Andrié, C., Leuenberger, M., Ludin, A., Raynaud, D., and Stauffer, B.: The age of the air in the firn and the ice at Summit, Greenland, Journal of Geophysical Research: Atmospheres, 98, 2831–2838, http://dx.doi.org/10.1029/92jd02383, 1993.

Severinghaus, J. P., Grachev, A., and Battle, M.: Thermal fractionation of air in polar firn by seasonal temperature gradients, Geochem. Geophy. Geosy., 2, 1048, doi:10.1029/2000GC000146, 2001.

Severinghaus, J. P., Albert, M. R., Courville, Z. R., Fahnestock, M. A., Kawamura, K., Montzka, S. A., Mühle, J., Scambos, T. A., Shields, E., Shuman, C. A., Suwa, M., Tans, P., andWeiss, R. F.: Deep air convection in the firn at a zero–accumulation site, central Antarctica, Earth Planet. Sc. Lett., 293, 359–367, https://doi.org/10.1016/j.epsl.2010.03.003, 2010.

Sowers, T., Bender, M., Raynaud, D., and Korotkevich, Y. S.: Delta n–15 of n2 in air trapped in polar ice – a tracer of gas–transport in the firn and a possible constraint on ice age–gas age–

differences, J. Geophys. Res.-Atmos., 97, 15683-15697, 1992.

Trudinger, C. M., Enting, I. G., Etheridge, D. M., Francey, R. J., Levchenko, V. A., Steele, L. P., Raynaud, D., and Arnaud, L.: Modeling air movement and bubble trapping in firn, J. Geophys. Res.-Atmos., 102, 6747-6763, doi:10.1029/96JD03382, 1997.

Witrant, E., Martinerie, P., Hogan, C., Laube, J. C., Kawamura, K., Capron, E., Montzka, S. A., Dlugokencky, E. J., Etheridge, D., Blunier, T., and Sturges, W. T.: A new multi-gas constrained model of trace gas non-homogeneous transport in firn: evaluation and behaviour at eleven polar sites, Atmos. Chem. Phys., 12, 11465-11483, doi:10.5194/acp-12-11465-2012, 2012.

Yang, J. W., Ahn, J., Brook, E. J., and Ryu, Y.: Atmospheric methane control mechanisms during the early Holocene, Climate of the Past, 13, 1227-1242, http://dx.doi.org/10.5194/cp-13-1227-2017, 2017.

Yang, J. W., Han, Y., Orsi, A. J., Kim, S. J., Han, H., Ryu, Y., Jang, Y., Moon, J., Choi, T., Hur, S. D., and Ahn, J.: Surface temperature in twentieth century at the Styx Glacier, northern Victoria Land, Antarctica, from borehole thermometry. Geophysical Research Letters., 2018.

Table 1. Glaciological characteristics of Styx Glacier and other firn air sampling sites.

Site	T (℃)	A (cm ice yr^{-1})	Firn air age (year)	LID (m)	COD (m)	LIZ thickness (m)	References
Styx	−31.7	10	89	52.4	64.8	12.4	This study, Yang et al. (2018)
Megadunes	−49	~0	121	64.5	68.5	4	Severinghaus et al. (2010)
South Pole	−51.0	8	93	115	125	10	Severinghaus et al. (2001)
Siple Dome	−25.4	13	55	49	58	9	Severinghaus et al. (2001)
Dome C	−54.5	2.7	30	97	100	3	Landais et al. (2006)
WAIS Divide	−31	22	38	~67	76.5	9.5	Battle et al. (2011)
NEEM	−28.9	22	48	63	78	15	Buizert et al. (2012a)
NGRIP	−31.1	19	45	67.5	78	11.5	Kawamura et al. (2006)
Summit	−32	23	27	70	80.8	10.8	Witrant et al. (2012)

Table 2. Comparison of standard deviation of density (σ_ρ) at critical density (ρ_{crit}). For data from all other sites, except the Styx, refer to Hörhold et al. (2011).

Campaign/Region	Core name	ρ_{crit} (kg m^{-3})	σ_ρ, ρ_{crit} (kg m^{-3})	T (℃)	A(cm ice yr^{-1})	σ_ρ, ρ_{crit} / A
Styx	Styx	821.68	19.33±1.87	−31.7	10	1.93±0.19
NGT	B16	819.27	12.26	−27	15.5	0.79
NGT	B18	820.81	12.81	−30	11.3	1.13
NGT	B21	820.81	12.91	−30	11.8	1.09
NGT	B26	820.85	13.23	−30.6	20	0.66
NGT	B29	821.32	10.50	−31.6	16.7	0.63
Berkner Island	B25	819.16	14.57	−27	15	0.97
DML	B31	827.00	10.27	−42	6.9	1.49
DML	B32	827.00	11.28	−42	6.7	1.68
DML	B36/37	827.50	8.12	−44.6	7.3	1.11
Pre−IPICS	B38	815.00	16.59	−18.1	136	0.12
Pre−IPICS	B39	814.91	17.11	−17.9	84	0.20
Pre−IPICS	DML95	815.51	13.42	−19.2	60	0.22
Pre−IPICS	DML97	816.07	10.03	−20.4	53	0.19
Dome C	EDC2	832.02	4.59	−53	2.7	1.70
WAIS Divide	WDC06A	820.81	10.35	−31	22	0.47

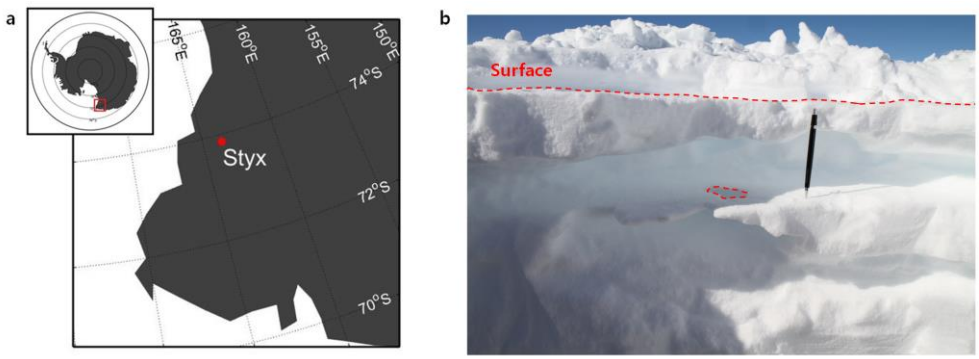

Figure 1. Location map of study site, Styx Glacier, Antarctica (a) and a photo of surface snow density layers (b). The thickness of snow density layers vary horizontally. The top boundaries of high-density layers are sharp (horizontal red-dashed line). A hole on a high-density layer surface is indicated by a red-dashed circle.

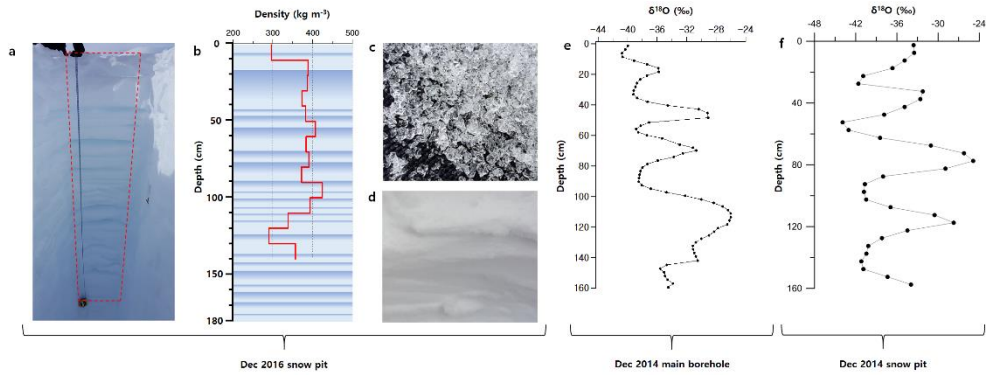

Figure 2. The snow-pit photos at Styx Glacier. (a) The snow-pit with dimensions of 280×65×220 cm (length×width×height). (b) The illustration of qualitatively-defined hard (high-density) and soft (low-density) layers with a 10 cm-resolution density profile. (c) Coarse grains observed in a soft layer. (d) Fine grains observed in a hard layer. Stable isotope ratio ($\delta^{18}O$) of snow profiles at the main core (e) and a snow-pit 100 m away from the main ice core borehole (f).

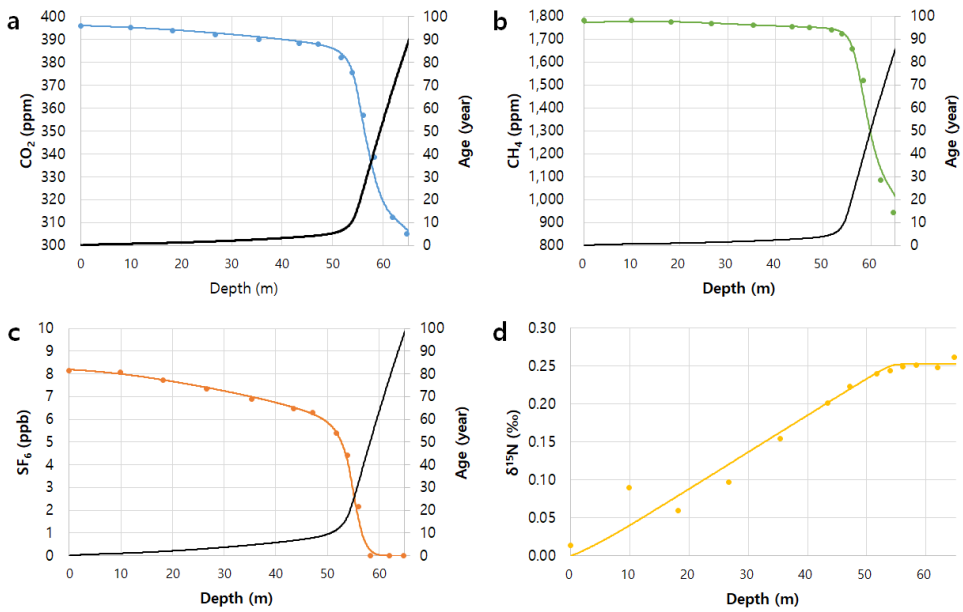

Figure 3. CO_2, CH_4, SF_6 mole fractions and $\delta^{15}N$ of N_2 measurements (circles), and model results (solid line) for the Styx firn air (air in open porosity). Black lines are modeled ages for the gas species.

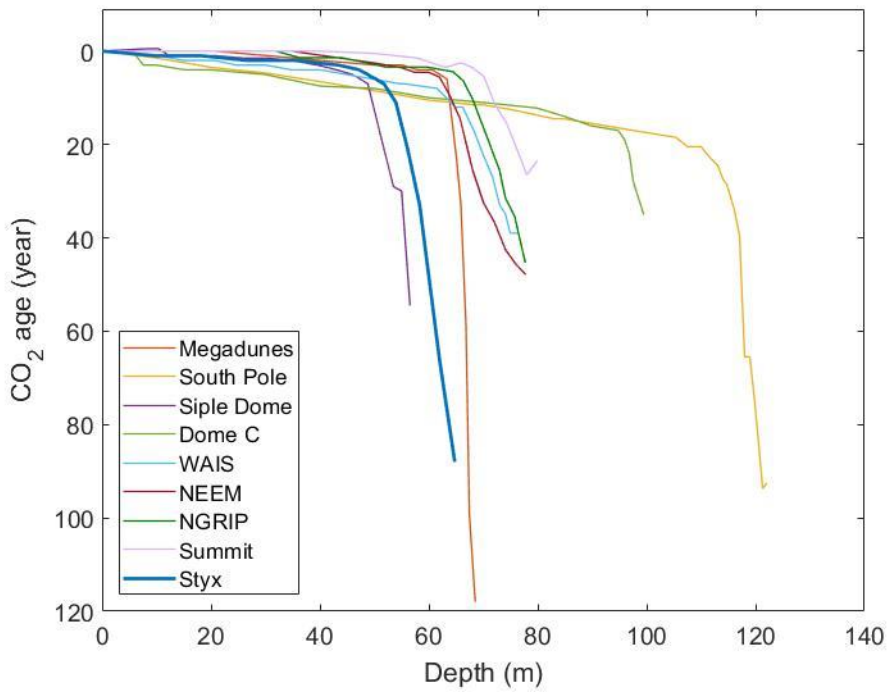

Figure 4. Comparison of CO_2 ages at several firn air sampling sites in Antarctica and Greenland. Old firn air (>55 years) is reported only in inland sites, where temperatures and snow accumulation rates are relatively low. However, 89-year old firn air was observed at Styx Glacier, where coast is near and snow accumulation rates are high.

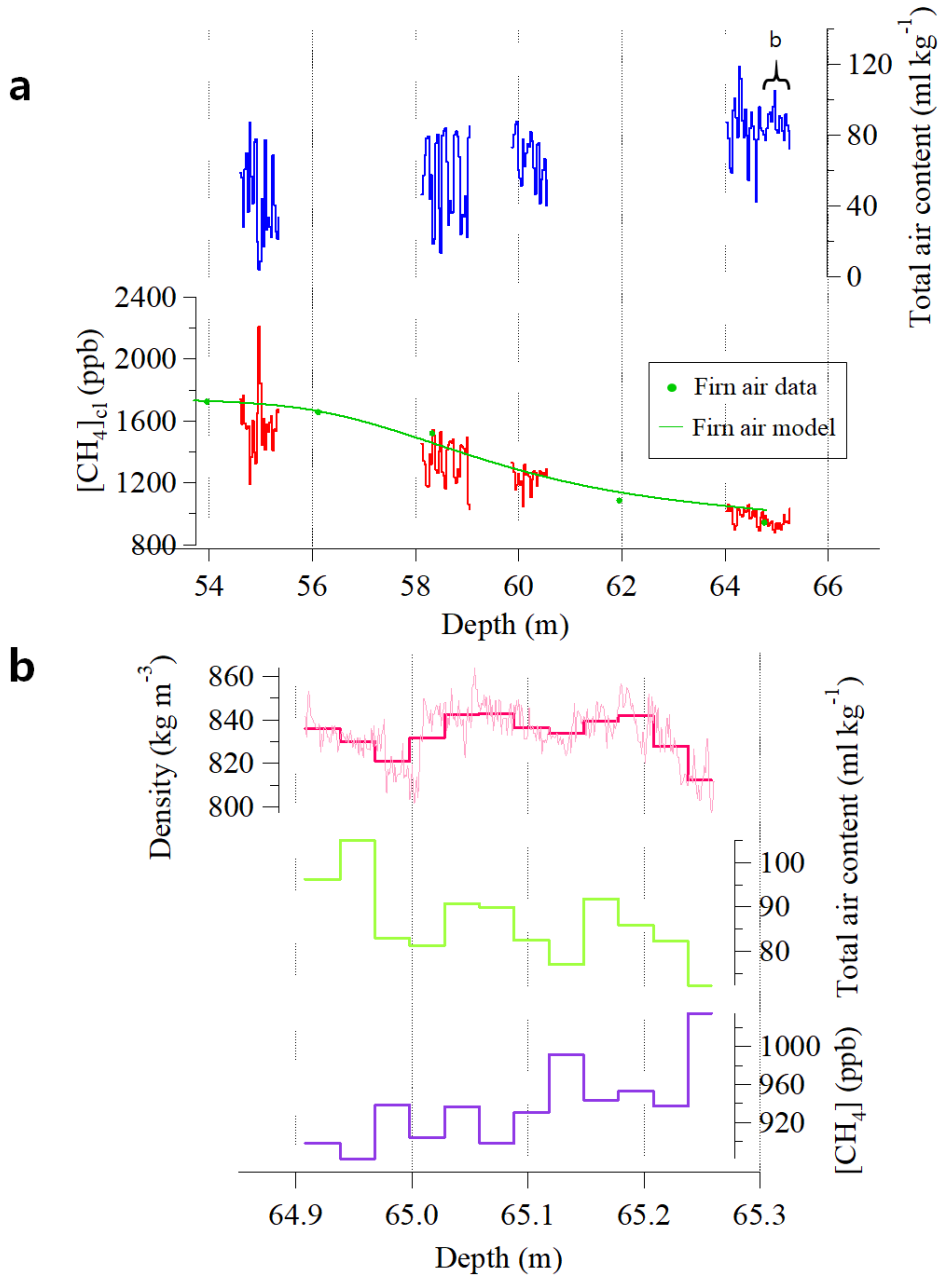

Figure 5. (a) CH_4 mole fraction in closed pores ($[CH_4]_{cl}$) (red line) and total air content (air volume per ice weight) (blue line) in the lock-in zone. Green line indicates CH_4 mole fraction in open pores. (b) Comparison of density with $[CH_4]_{cl}$ and total air content near COD.

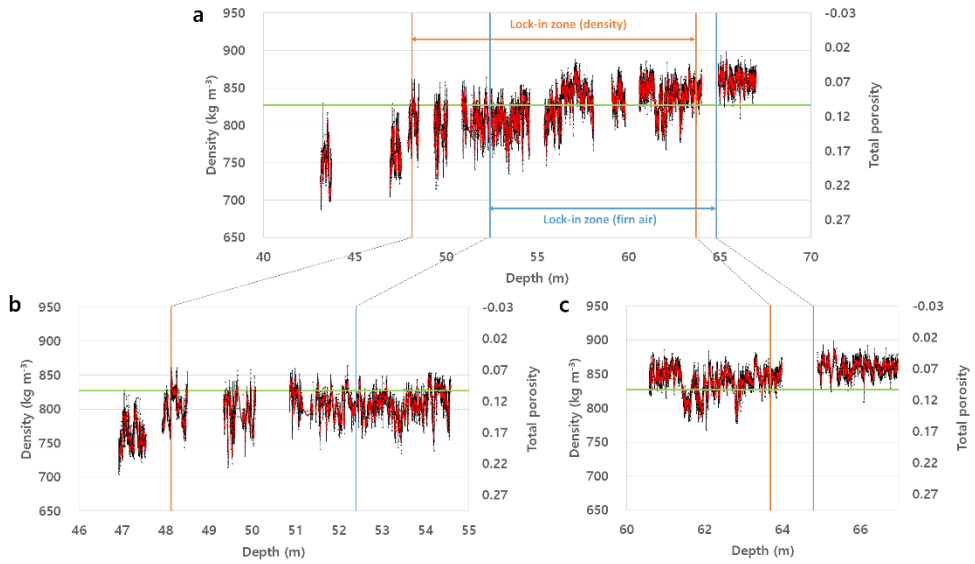

Figure 6. X-ray high-resolution density data obtained from the lock-in zone. (b) and (c) are enlarged portion of (a). Black lines show individual density data, while the red lines 1-cm running means. Blue and orange lines represent the boundaries of the LIZ estimated from the gas compositions (between two vertical blue lines) and the critical porosity measurements (between two orange vertical lines), respectively.

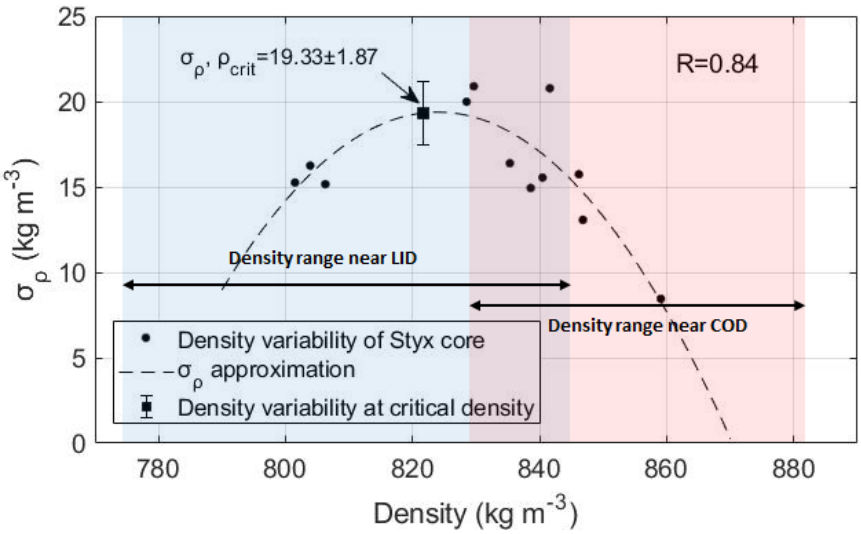

Figure 7. Density variability calculated from 1000 depth points and their average density. The standard deviation at the critical density (821.68 kg m^{-3}) calculated from the approximate secondary equation (R=0.84) is 19.33±1.87 kg m^{-3}. The blue and red areas are the density ranges near the LID (52.38–52.48 m) and the COD (64.91–65.01 m), respectively.

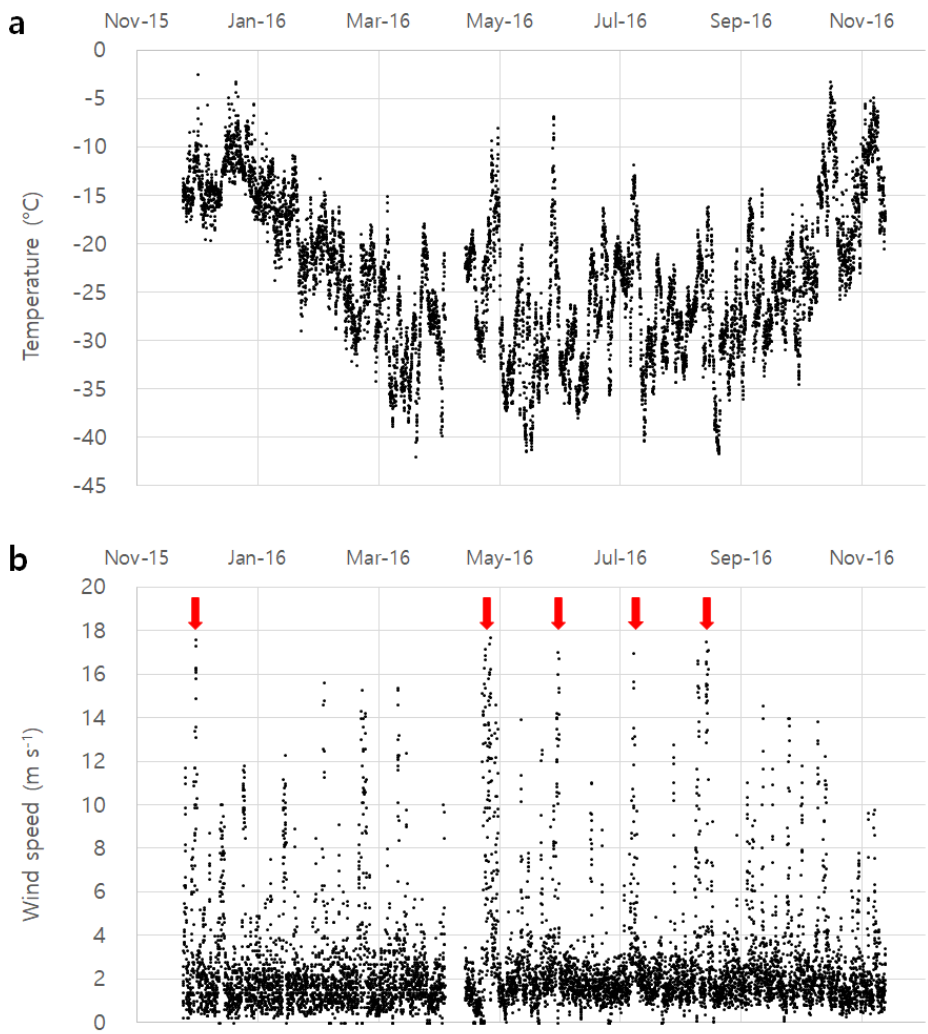

Figure 8. Surface air temperature (a) and wind speed (b) data from AWS (Automatic Weather System) at Styx Glacier during December 2015 to December 2016. Red arrows indicate blizzard events.

국문초록

펀 공기(Firn air)는 비교적 최근 과거의 공기를 다량으로 제공하기 때문에 인간활동에 의한 대기 조성 변화를 이해하는 데 유용하게 사용될 수 있다. 기존에 연구된 대부분의 펀 공기 기록은 지난 수십 년(일반적으로 40 년에서 55 년)에 해당되며, 이는 인간이 대기에 영향을 미치기 시작한 초기 부분을 다루기에는 불충분하다. 이와 반대로, 온도와 적설량이 매우 낮은 내륙지역의 일부 펀 공기 자료는 약 한 세기 전까지의 펀 공기를 보존하고 있다. 이 연구에서 우리는 남극 로스해 연안 인근의 스틱스 빙하로부터 약 89 년에 해당되는 오래된 펀 공기를 발견하였다. 이는 비교적 따뜻한 연안 지역에서 오래된(60 년 이상) 펀 공기를 발견한 첫 번째 연구이다. 스틱스 빙하의 또 다른 특징으로 잠금구간(Lock-in zone)의 두께는 12.4 m 로 비슷한 온도와 적설량을 갖는 다른 지역에 비해 두꺼웠다. 그 원인을 알기 위해 고해상도 X-선 밀도측정을 수행했고, 스틱스 빙하의 높은 밀도 변동성을 확인하였다. 닫힌 공극 속의 메탄의 몰분율과 총 공기함량 또한 cm 규모에서 큰 변동성을 지시하고, 이는 밀도층(Layering)을 의미한다. 우리는 펀에서의 큰 밀도 변동성이 잠금구간의 두께를 증가시키고 결과적으로 펀 공기의 연령을 증가시킨다는 가설을 세웠다. 왜냐하면 펀 공기의 연령은 잠금구간에서 깊이에 따라 급격하게 증가하기 때문이다. 우리의 연구는 비록 온도와 적설량이 상대적으로 높더라도, 밀도 변동성이 잘 발달되기 유리한 기상조건을 갖는 지역에서는 더 오래된 펀 공기가 보존됨을 보여주었다.

주요어 : 펀 공기 연령, 밀도, 층, 메탄

학번 : 2016-20426

Appendix

A1. Firn air sampling procedure

The preparation process before firn air sampling is as follows:

1) Setting up the firn air sampling tent

   The firn air sampling tent at Styx Glacier in 2014–2015 season was located about 10 m southwest of the drilling tent and was set up more than 100 m north of the main camp to prevent the contamination from the generator and human respiration.

2) Assembling the bladder

   The assembly order of the bladder were (1) connecting the top part and the tubings, (2) connecting the bottom part and the tubings, and (3) connecting the bladder rubber and the top/bottom parts.

3) Leak check

   The leak check in the bladder and the pumping line was conducted with pressure gauges in the air pumping system box.

4) Calibrating LI–COR for CO_2 analysis

   Daily LI–COR calibration was performed using two CO_2 standard airs before the first air sampling.

5) Bladder pressurization test

   This is the test that how much pressure is needed to inflate the bladder and prevent air leak through the borehole.

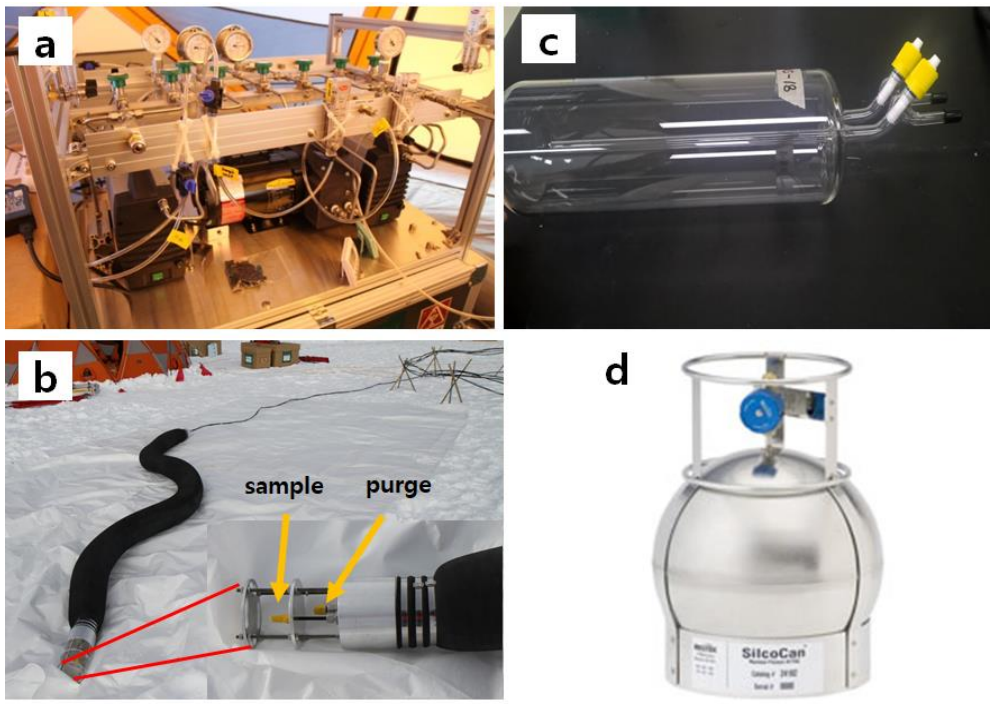

Figure A1. The firn air sampling devices. (a) Pumping system. (b) Rubber bladder system. The figure insert is the enlargement portion of the bladder bottom part. (c) Glass flask. (d) Stainless steel silcocan canister.

Table A1. CO_2, CH_4, SF_6 mole fractions and $\delta^{15}N$ of N_2 of the firn air collected from the Styx Glacier.

Depth (m)	CO_2 (ppm)	CH_4 (ppb)	SF_6 (ppt)	$\delta^{15}N$ of N_2 (‰)
0.00	395.78	1780.6	8.2	0.014
9.90	395.35	1781.4	8.1	0.090
18.21	393.84	1776.5	7.7	0.060
26.68	392.25	1768.0	7.4	0.098
35.36	390.16	1759.8	6.9	0.154
43.42	388.42	1754.9	6.5	0.201
47.21	387.90	1752.5	6.3	0.224
51.75	382.15	1741.0	5.4	0.240
53.95	375.70	1724.8	4.4	0.244
56.11	356.89	1656.6	2.2	0.249
58.32	338.52	1520.1	0.0	0.251
61.95	312.35	1085.9	0.0	0.249
64.76	305.18	943.4	0.0	0.262

Table A2. Comparison of CO_2 and CH_4 concentrations between airs in Silcocan canisters and glass flasks.

Depth (m)	Silcocan Canister		Glass Flask		Difference (Glass − Silcocan)	
	CO_2 (ppm)	CH_4 (ppb)	CO_2 (ppm)	CH_4 (ppb)	CO_2 (ppm)	CH_4 (ppb)
0	397.03	1780.5	395.78	1780.6	−1.25	0.1
35.36	390.45	1758.6	390.16	1759.8	−0.29	1.2
43.42	388.65	1754.3	388.42	1754.9	−0.23	0.6
53.95	375.69	1725.3	375.7	1724.8	0.01	−0.5

Table A3. Sampling information.

	Flask No.	Date (yy/mm/dd)	Depth (m)		Bladder pressure	sample air venting			CO2 conc.		Sample container flushing	
			Drilling depth	Firn tubing depth		start time	flow rate	end time	purge	sam. vent.	flow rate	duration
LI-COR calibration	S-02	2014-12-12	-	현생대기	-	20:42	10L/min	20:59	397.5ppm	-	5.0L/min	20min
	S-06	2014-12-12	9.9m	9.90m	over 0.21bar	23:24	9L/min	23:49	397.0ppm	-	5.0L/min	41min
	S-05	2014-12-13	18.21m	18.295m	over 0.20bar	4:33	9L/min	4:43	394.0ppm	-	5.0L/min	20min
	S-20	2014-12-13	18.21m	18.295m	over 0.20bar	5:17	9L/min	5:26	394.0ppm	-	5.0L/min	20min
	SSC-1	2014-12-13	-	현생대기	-	8:13	9L/min	8:34	396.2ppm	-	comments	22min
	S-32	2014-12-13	26.68m	27.02m	over 0.35bar	21:52	9L/min	22:00	392.5ppm	-	5.0L/min	20min
offset check +0.2ppm	~~S-28~~	~~2014-12-14~~	~~35.36m~~	-	~~over 0.35bar~~	~~3:00~~	~~9L/min~~	~~3:19~~	~~391.8ppm~~	-	~~5.0L/min~~	~~20min~~
	SSC-2	2014-12-14	35.36m	-	over 0.20bar	3:45	9L/min	4:05	390.8ppm	-	comments	20min
	S-28	2014-12-14	35,36m	-	over 0.35bar	4:14	9L/min	4:24	390.6ppm	-	5.0L/min	20min
	S-27	2014-12-14	43.42m	44.07m	over 0.35bar	8:27	9L/min	8:38	387.3ppm	-	5.0L/min	32min
	SSC-3	2014-12-14	43.42m	44.07m	over 0.35bar	9:21	9L/min	9:42	387.3ppm	-	comments	20min
offset check +2.0ppm	S-19	2014-12-14	47.21m	47.86m	over 0.4bar	23:28	9L/min	23:40	388.6ppm	-	5.0L/min	20min
	S-31	2014-12-15	47.21m	47.86m	over 0.4bar	0:05	9L/min	0:35	388.6ppm	-	5.0L/min	35min
	S-24	2014-12-15	51.75m	52.51m	over 0.4bar	3:41	9L/min	3:51	385.2ppm	-	5.0L/min	20min
	C-01	2014-12-15	53.95m	54.71m	over 0.4bar	6:01	9L/min	6:11	376.7ppm	-	5.0L/min	20min
	SSC-4	2014-12-15	53.95m	54.71m	over 0.42bar	6:41	9L/min	7:02	376.7ppm	-	comments	21min
	C-02	2014-12-15	-	현생대기	-	10:09	9L/min	10:24	395.8ppm	-	5.0L/min	20min
	SSC-5	2014-12-15	-	현생대기	-	10:51	9L/min	11:35	395.7ppm	-	comments	42min
offset check +2.4ppm	S-03	2014-12-15	56.11m	57.12m	over 0.4bar	21:38	9L/min	21:51	360.9ppm	-	5.0L/min	25min
	S-22	2014-12-16	58.32m	59.24m	over 0.4bar	0:07	9L/min	0:17	340.5ppm	-	5.0L/min	30min
	S-07	2014-12-16	61.95m	63.01m	over 0.4bar	3:14	9L/min	3:42	313.6ppm	-	4.8L/min	20min
	S-04	2014-12-16	64.76m	65.80m	over 0.4bar	6:23	3.5L/min	6:34	307.0ppm	-	2.0L/min	20min
	S-18	2014-12-16	66.81m	68.26m	over 0.4bar							
			66.31m	0.5m올림	over 0.2bar	9:02						
			65.81m	0.5m올림	over 0.25bar	9:16						
			65.41m	0.4m올림	over 0.25bar	9:28	1.5L/min					
			65.11m	0.3m올림	over 0.25bar							
	SSC-6	2014-12-17	-	현생대기	-	13:14	9L/min	13:44	396.3ppm	-	comments	45min

	Flask No.	air pressure in flask	CO2 conc.		End time	Comments
			purge	sam. vent.		
LI-COR calibration	S-02	over 1.0bar	397.5ppm	-	21:21	현생대기 샘플링, 3분간 샘플 플라스크 진공 후 -0.85 bar/ 2분후 체크했을 때 -0.85 bar. 샘플 플라스크 IN측 입구에 Mg(ClO4)2 들어감. 샘플 측정시 유의할 것.
	S-06	over 1.0bar	397.0ppm	-	0:45	처음에 S-01 플라스크를 이용하려다가 leak이 발견되어 S-06 플라스크를 이용하였음. 2014/12/13 00:45 에 종료됨.
	S-05	over 1.0bar	394.1ppm	-	5:16	플라스크 입구가 열려있어서, DIA-2 펌프를 이용하여 120분간 진공시킨 후 이용하였음. 진공시킨 다음에 밸브를 잠근 직후: -0.84bar, 2분후 : -0.84bar
	S-20	over 1.0bar	394.1ppm	-	5:53	플라스크 입구가 열려있어서, DIA-2 펌프를 이용하여 10분간 진공시킨 후 이용하였음.
	SSC-1	over 2.0bar	396.0ppm	-	8:59	sample container flushing method : evacuate + { 3 * (fill + evacuate) }
	S-32	over 1.0bar	392.5ppm	-	22:26	
offset check +0.2ppm	~~S-28~~	~~over 1.0bar~~	~~391.1ppm~~	-	~~3:40~~	샘플 채집 전에 standard air를 이용하여 LI-COR 드래프트 체크하였음. 그 결과, 302.9ppm 나옴(실제 농도는 302.7ppm). /// CO2 안정화 되기 전에 샘플링 한것으로 판단 되어 다시 샘플링 하도록 하였음.
	SSC-2	over 2.0bar	390.7ppm	-	4:10	CO2를 안정화 시키는데 50분 이상 걸렸음. CO2 농도가 안정화 되는데 오래 걸린 이유는 "블래더를 중간에 멈추지 않고 계속 내리기만 하였기 때문"으로 생각됨. sample container flushing method : evacuate + { 2 * (fill + evacuate) }
	S-28	over 1.0bar	390.6ppm	-	4:50	같은 날 오전 3시 00분부터 S-28 플라스크로 채집한 firn air를 vacuum 한 후에 다시 채집한 것임.
	S-27	over 1.0bar	387.3ppm	-	9:13	플라스크 입구가 열려있어서, DIA-2 펌프를 이용하여 187분간 진공시킨 후 이용하였음.
	SSC-3	over 2.0bar	387.4ppm	-	9:47	sample container flushing method : evacuate + { 2 * (fill + evacuate) }
offset check +2.0ppm	S-19	over 1.0bar	388.6ppm	-	0:03	플라스크 입구가 열려있어서, DIA-2 펌프를 이용하여 128분간 진공시킨 후 이용하였음.
	S-31	over 1.0bar	388.6ppm	-	1:14	플라스크 입구가 열려있어서, DIA-2 펌프를 이용하여 26분간 진공시킨 후 이용하였음.
	S-24	over 1.0bar	385.2ppm	382.7ppm	4:20	플라스크 입구가 열려있어서, DIA-2 펌프를 이용하여 149분간 진공시킨 후 이용하였음.
	C-01	over 1.0bar	376.7ppm	375.7ppm	6:36	플라스크 입구가 열려있어서, DIA-2 펌프를 이용하여 105분간 진공시킨 후 이용하였음.
	SSC-4	over 2.0bar	376.6ppm	375.5ppm	7:11	sample container flushing method : evacuate + { 2 * (fill + evacuate) }
	C-02	over 1.0bar	395.7ppm	-	10:50	플라스크 입구가 열려있어서, DIA-2 펌프를 이용하여 88분간 진공시킨 후 이용하였음.
	SSC-5	over 2.0bar	395.7ppm	-	11:40	sample container flushing method : evacuate + { 2 * (fill + evacuate) }
offset check +2.4ppm	S-03	over 1.0bar	359.8ppm	-	22:20	플라스크 입구가 열려있어서, DIA-2 펌프를 이용하여 96분간 진공시킨 후 이용하였음.
	S-22	over 1.0bar	340.5ppm	339.7ppm	0:54	플라스크 입구가 열려있어서, DIA-2 펌프를 이용하여 112분간 진공시킨 후 이용하였음.
	S-07	over 1.0bar	313.2ppm	313.0ppm	4:06	플라스크 입구가 열려있어서, DIA-2 펌프를 이용하여 164분간 진공시킨 후 이용하였음.
	S-04	over 1.0bar	306.7ppm	305.4ppm	7:01	플라스크 입구가 열려있어서, DIA-2 펌프를 이용하여 140분간 진공시킨 후 이용하였음.
	S-18					펌프로 공기를 뽑아낼 수 없었음.
						펌프로 공기를 뽑아낼 수 없었음.
						펌프로 공기를 뽑아낼 수 없었음.
						처음에는 펌프로 공기를 뽑아낼 수 있었으나, 시간이 지난 후 flow rate이 0에 가까워서 샘플링하지 못함.
						처음에는 펌프로 공기를 뽑아낼 수 있었으나, 시간이 지난 후 flow rate이 0에 가까워서 샘플링하지 못함.
	SSC-6	over 2.0bar	395.7ppm	-	14:40	sample container flushing method : evacuate + { 2 * (fill + evacuate) }

A2. Physical properties of firn at Styx Glacier

The Styx Glacier has a distinct layers in the firn layer compared to other ice core sites. Density of the upper snow layer were measured for a basic survey of its causes. A 2.2 m – deep snow pit was dug out with shovels, and the density cutter were used to collect a 1L snow specimen and measure its density. The density were calculated using this equation:

$$\rho = (M_{snow+density\ \ cutter} - M_{density\ \ cutter})/V$$

where M is a mass and V is a volume of snow. $M_{\text{density cutter}}$ is 1238 ± 1 g, and V is 1 L. We also were able to distinguish between rigid and soft layers by hand scraping the snow wall.

Table A4. 10 cm-resolution density data.

Top depth (cm)	Bottom depth (cm)	Middle depth (cm)	Density (kg/m^3)
0	10	5	296
10	20	15	389
20	30	25	387
30	40	35	373
40	50	45	383
50	60	55	407
60	70	65	384
70	80	75	391
80	90	85	372
90	100	95	424
100	110	105	394
110	120	115	338
120	130	125	290
130	140	135	357

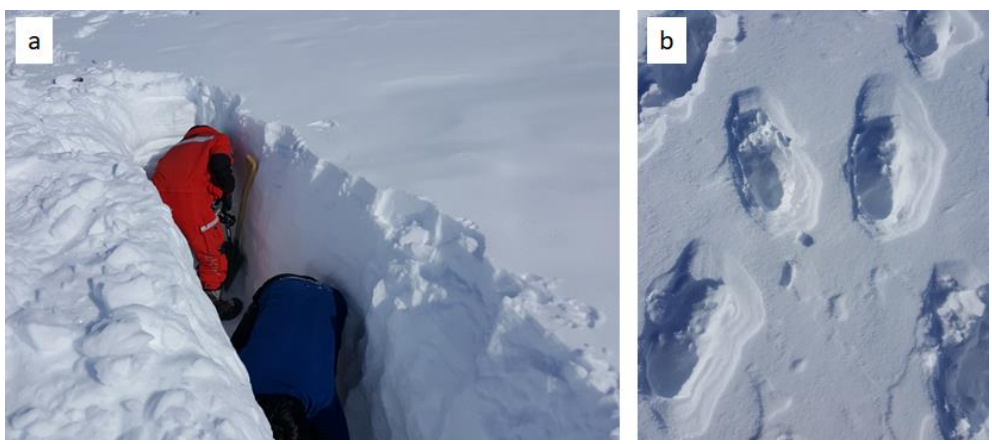

Figure A2. (a) The snow pit, and (b) footprints on the surface

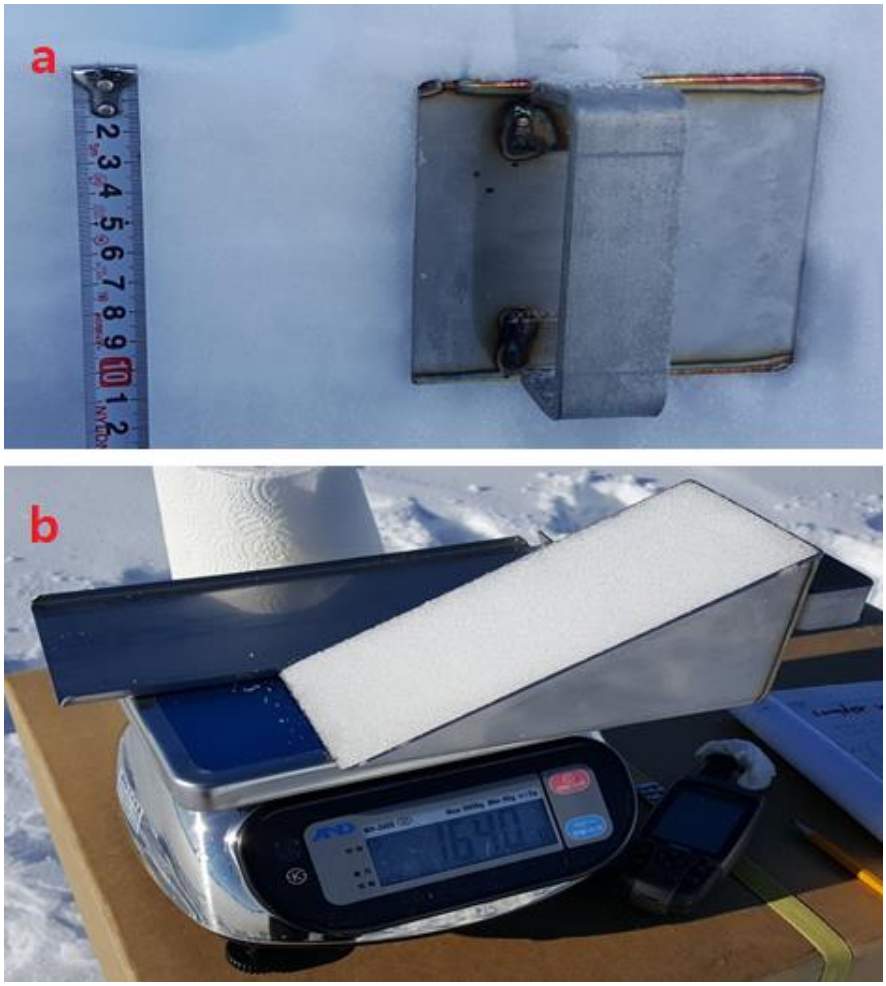

Figure A3. Pictures of measuring surface snow density

A3. Firn analysis

Firn ice has a low density and a high porosity because it is less densified than the mature ice. It is difficult to precisely analyze greenhouse gas concentrations for extracted air from the firn ice compared to the mature ice because of the small quantity of air trapped in the closed pores.

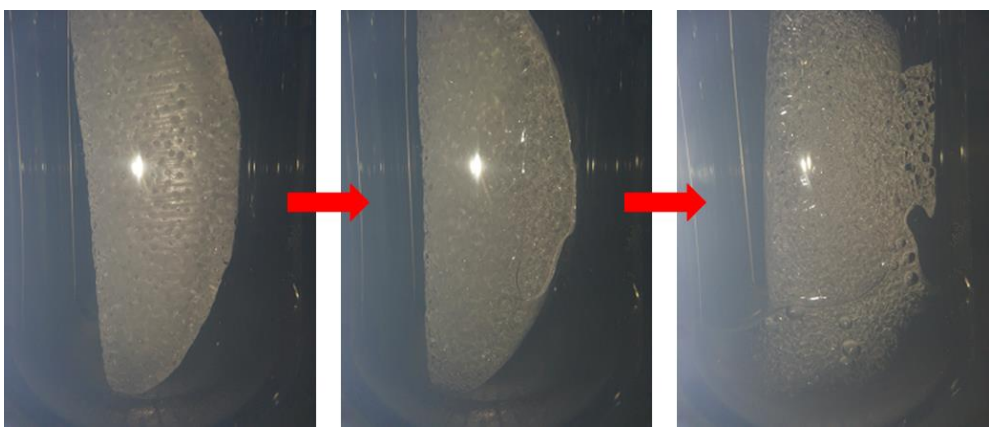

Figure A4. The firn ice sample melting in the glass flask in order to reduce cutting loss as much as possible, the firn ice were cut as its original shape (semicircular).

Table A5. CH_4 mole fractions and total air content.

Top Depth (m)	Bottom Depth (m)	Middle Depth (m)	CH_4 (ppb)	Air content (ml kg^{-1})
54.575	54.605	54.59	1742	58.6
54.605	54.635	54.62	1579	55.8
54.635	54.665	54.65	1764	27.9
54.665	54.695	54.68	1586	60.9
54.695	54.725	54.71	1549	69.9
54.725	54.755	54.74	1568	36.5
54.755	54.785	54.77	1191	87
54.785	54.815	54.8	1364	56.7
54.815	54.845	54.83	1602	41.4
54.845	54.875	54.86	1398	76.2
54.875	54.905	54.89	1325	77.8
54.905	54.935	54.92	1648	19.6
54.935	54.965	54.95	2209	3.7
54.965	54.995	54.98	1844	8.7
54.995	55.025	55.01	1444	43.9
55.025	55.055	55.04	1615	17.1
55.055	55.085	55.07	1413	77.2
55.085	55.115	55.1	1578	26.4
55.115	55.145	55.13	1531	33.6
55.145	55.175	55.16	1590	28.1
55.175	55.205	55.19	1632	22.4
55.205	55.235	55.22	1409	68.7
55.235	55.265	55.25	1546	40.5
55.265	55.295	55.28	1538	25.5
55.295	55.325	55.31	1673	21.4
55.325	55.355	55.34	1655	33.3
58.096	58.126	58.111	1453	46.5
58.126	58.156	58.141	1342	57.1
58.156	58.186	58.171	1319	68.7
58.186	58.216	58.201	1181	78.3
58.216	58.246	58.231	1175	79.5
58.246	58.276	58.261	1386	44.2
58.276	58.306	58.291	1321	57.4
58.306	58.336	58.321	1544	18.5
58.336	58.371	58.3535	1505	21.2
58.371	58.401	58.386	1285	75.8
58.401	58.431	58.416	1264	80.3
58.431	58.461	58.446	1400	38.8
58.461	58.491	58.476	1531	13.6
58.491	58.521	58.506	1268	79.6
58.521	58.551	58.536	1250	82.3

Top Depth (m)	Bottom Depth (m)	Middle Depth (m)	CH_4 (ppb)	Air content (ml kg^{-1})
58.551	58.581	58.566	1164	83.8
58.581	58.611	58.596	1414	64.8
58.611	58.641	58.626	1443	29.4
58.641	58.671	58.656	1471	42.8
58.671	58.701	58.686	1460	35.9
58.701	58.731	58.716	1479	36.4
58.731	58.761	58.746	1237	80.4
58.761	58.791	58.776	1199	82.2
58.791	58.821	58.806	1290	79.2
58.821	58.851	58.836	1242	67.5
58.851	58.881	58.866	1442	24.1
58.881	58.911	58.896	1436	35.1
58.911	58.941	58.926	1423	33.8
58.941	58.971	58.956	1386	45.3
58.971	59.001	58.986	1496	22.3
59.001	59.031	59.016	1060	78.5
59.031	59.061	59.046	1028	85.3
59.847	59.877	59.862	1330	73.1
59.877	59.907	59.892	1270	80.5
59.907	59.937	59.922	1155	86.3
59.937	59.967	59.952	1189	87.6
59.967	59.997	59.982	1261	60.5
59.997	60.027	60.012	1185	55.5
60.027	60.057	60.042	1211	51.3
60.057	60.087	60.072	1046	77.7
60.087	60.117	60.102	1316	62.1
60.117	60.147	60.132	1253	69.9
60.147	60.177	60.162	1263	75
60.177	60.207	60.192	1242	73.6
60.207	60.237	60.222	1105	81.8
60.237	60.267	60.252	1220	76.5
60.267	60.297	60.282	1276	61.4
60.297	60.327	60.312	1265	46.8
60.327	60.357	60.342	1177	74.7
60.357	60.387	60.372	1244	75.4
60.387	60.417	60.402	1277	41.3
60.417	60.447	60.432	1247	55
60.447	60.477	60.462	1263	60.4
60.477	60.507	60.492	1244	66.7
60.507	60.537	60.522	1290	40.2
60.537	60.567	60.552	12359	54.2
64.008	64.038	64.023	1016	87.3

Top Depth (m)	Bottom Depth (m)	Middle Depth (m)	CH_4 (ppb)	Air content (ml kg^{-1})
64.038	64.068	64.053	1060	78.4
64.068	64.098	64.083	1016	61.4
64.098	64.128	64.113	1046	58.8
64.128	64.158	64.143	935	93.8
64.158	64.188	64.173	897	100.8
64.188	64.218	64.203	922	90
64.218	64.248	64.233	1036	78.7
64.248	64.278	64.263	1023	118.9
64.278	64.308	64.293	993	112.1
64.308	64.338	64.323	982	88.1
64.338	64.368	64.353	1031	79
64.368	64.398	64.383	1010	94.7
64.398	64.428	64.413	1020	79.8
64.428	64.458	64.443	1057	54.4
64.458	64.488	64.473	967	84
64.488	64.518	64.503	974	93.1
64.518	64.548	64.533	1015	85.3
64.548	64.578	64.563	984	77.5
64.578	64.608	64.593	1017	42.1
64.608	64.638	64.623	913	77.5
64.638	64.668	64.653	889	95.9
64.668	64.698	64.683	976	84.0
64.698	64.728	64.713	1013	82.5
64.728	64.758	64.743	956	80.4
64.758	64.788	64.773	985	77.4
64.788	64.818	64.803	963	84.0
64.818	64.848	64.833	923	91.8
64.848	64.878	64.863	941	93.1
64.878	64.908	64.893	952	87.5
64.908	64.938	64.923	898	96.3
64.938	64.968	64.953	882	105
64.968	64.998	64.983	938	83
64.998	65.028	65.013	904	81.2
65.028	65.058	65.043	937	90.8
65.058	65.088	65.073	898	89.9
65.088	65.118	65.103	930	82.4
65.118	65.148	65.133	991	77
65.148	65.178	65.163	944	91.8
65.178	65.208	65.193	953	85.8
65.208	65.238	65.223	937	82.2
65.238	65.268	65.253	1035	72.2

Table A6. Stable isotope ratios of ice ($\delta^{18}O$ and δD).

Top Depth (m)	Bottom Depth (m)	Middle Depth (m)	n of analysis	$\delta^{18}O$	sd	δD	sd
58.096	58.126	58.111	2	−34.04	0.04	−267.8	0.0
58.126	58.156	58.141	1	−33.96		−268.1	
58.156	58.186	58.171	1	−34.01		−268.5	
58.186	58.216	58.201	1	−33.81		−267.5	
58.216	58.246	58.231	2	−33.44	0.01	−263.9	0.5
58.246	58.276	58.261	2	−33.16	0.04	−261.0	0.4
58.276	58.306	58.291	2	−32.78	0.05	−257.3	0.7
58.306	58.336	58.321	2	−32.62	0.02	−255.6	0.3
58.336	58.371	58.354	2	−32.49	0.01	−255.2	0.2
58.371	58.401	58.386	2	−32.68	0.01	−257.0	0.2
58.401	58.431	58.416	2	−33.06	0.07	−259.3	0.1
58.431	58.461	58.446	3	−33.45	0.07	−263.4	0.8
58.461	58.491	58.476	2	−33.58	0.07	−265.7	0.6
58.491	58.521	58.506	2	−34.05	0.01	−269.5	0.2
58.521	58.551	58.536	3	−34.27	0.10	−271.9	0.8
58.551	58.581	58.566	2	−34.34	0.07	−272.6	0.3
58.581	58.611	58.596	3	−33.97	0.14	−269.1	1.0
58.611	58.641	58.626	2	−33.64	0.01	−266.0	0.2
58.641	58.671	58.656	1	−33.55		−264.4	
58.671	58.701	58.686	1	−33.11		−261.1	
58.701	58.731	58.716	1	−33.25		−261.5	
58.731	58.761	58.746	2	−33.31	0.09	−262.5	0.8
58.761	58.791	58.776	1	−33.70		−265.5	
58.791	58.821	58.806	1	−34.03		−268.7	
58.821	58.851	58.836	1	−34.33		−271.5	
58.851	58.881	58.866	1	−34.47		−273.1	
58.881	58.911	58.896	1	−34.46		−273.2	
58.911	58.941	58.926	1	−34.56		−273.1	
58.941	58.971	58.956	1	−34.45		−272.2	
58.971	59.001	58.986	1	−34.47		−271.9	
59.001	59.031	59.016	1	−34.47		−272.3	
59.031	59.061	59.046	1	−34.59		−275.1	

A4. X-ray density measurement

The high-resolution density measurements were performed at Institute of Low Temperature Science, Hokkaido University. After trimming and polishing of ice surface, the firn ice sample was fixed at the analysis instrument in the freezer X-ray room. The sample was placed on the sample stage, and positioned the top direction at the beginning of the measurement. The detector on the opposite side of the source shows the intensity of the X-ray beam which is detected.

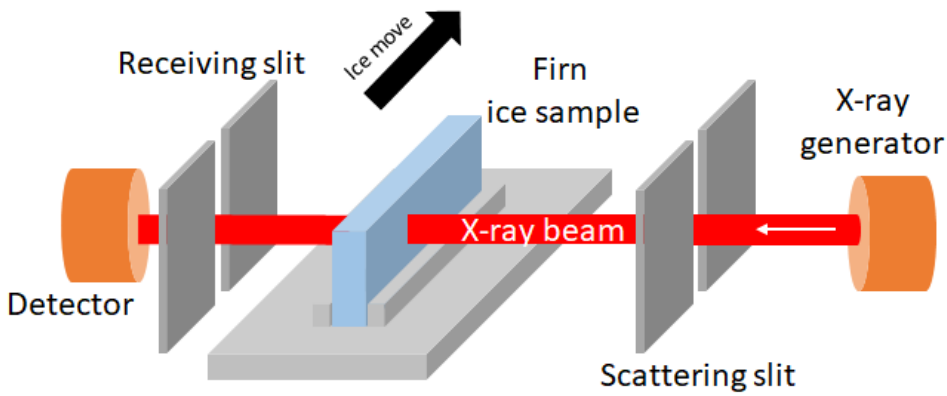

Figure A5. Schematic diagram of the X-ray transmission method. Modified from Hori et al. (1999).

A5. Firn air model results

The density and porosity of firn can be modeled by Center of Ice and Climate (CIC) firn air transport model. Total porosity is the sum of open porosity and closed porosity. The open porosity decreases continuously from the glacier surface, while the close porosity starts to increase near the beginning of the lock-in zone (LIZ).

Firn air at a certain depth does not show a single age, but have age distribution. The age distribution of firn air also can be modeled. As the depth increases, older age and wide range of the age are modeled. The average age is smaller than 10 years above 50 m. However, the firn air ages increases dramatically in the LIZ (Fig. A7).

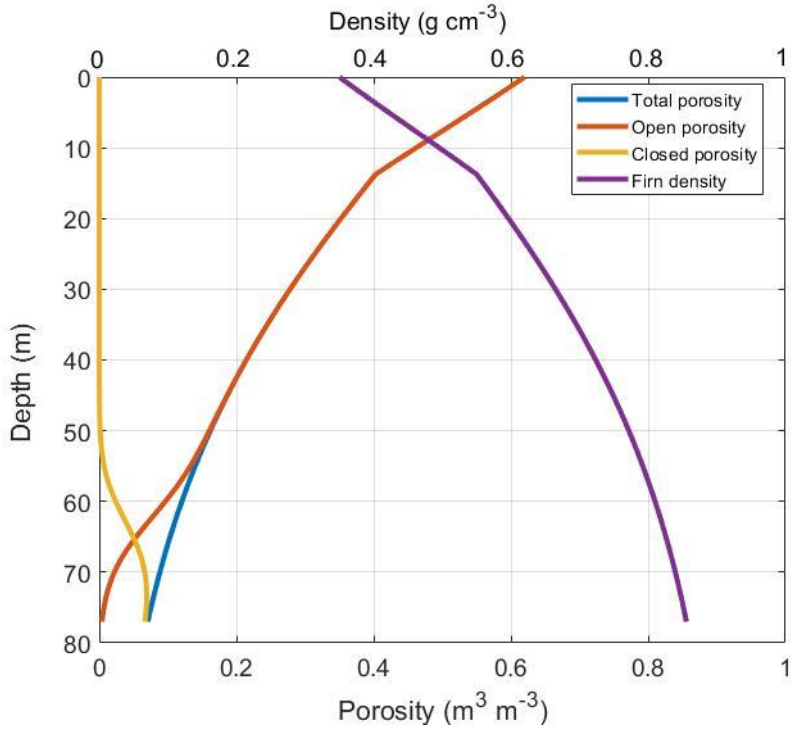

Figure A6. Firn density and porosity.

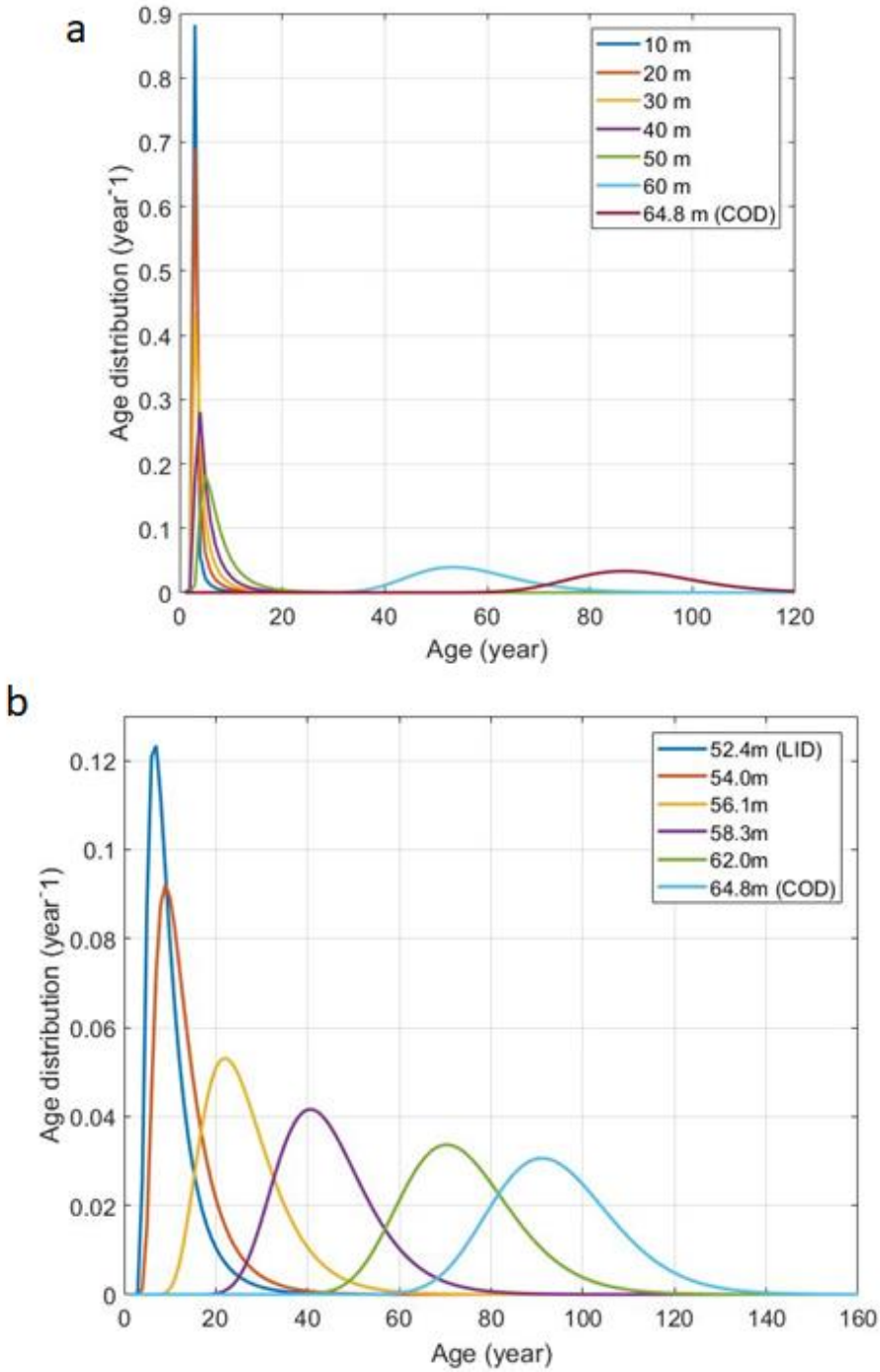

Figure A7. CO_2 age distribution.

A6. Implications from distribution of greenhouse gas concentrations in closed bubbles in the firn ice

We observed snow layers with different densities near the the surface of Styx glacier. The density variations were confirmed with analyses of CH_4 and total air content of firn ice. High-density firn layers may reach to lock-in and close-off at shallower depths than low-density layers. Thus, air bubbles might have trapped at shallower depths in high-density layers. Early trapped air may preserve old air with low greenhouse gas concentrations. Meanwhile, the high-density layers have small open porosity and large closed porosity. Thus, high air contents are expected at high-density layers. Snow density layers may prevent air transportation and increase thickness of LIZ as shown in WAIS Divide ice (Mitchell et al. 2015), making firn air older than non-layering sites.

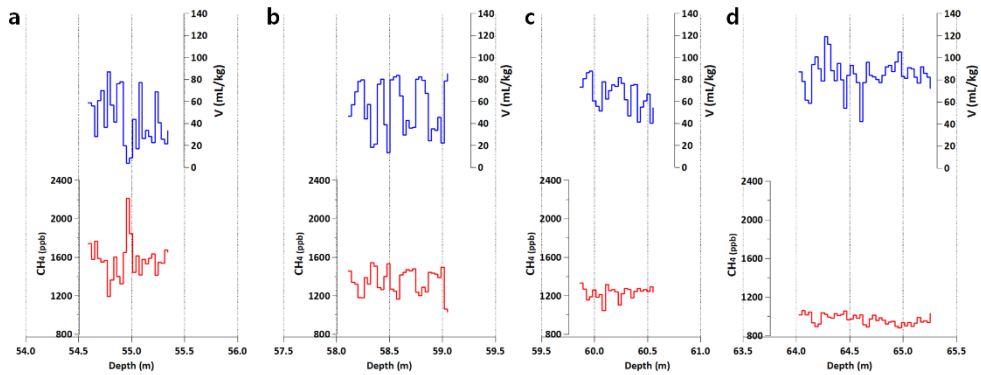

Figure A8. (a) ~ (d) CH_4 mole fraction (red) and total air content (air volume per ice weight) (blue) in the lock-in zone.

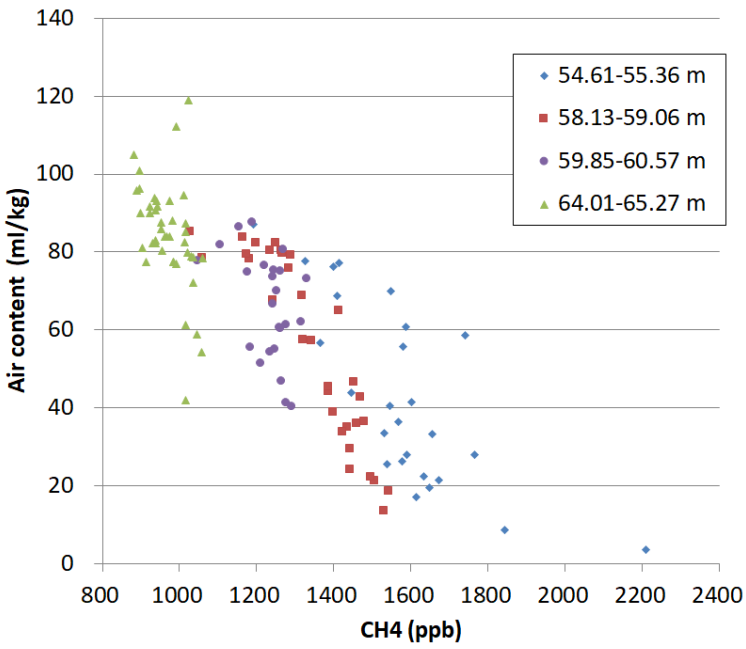

Figure A9. Comparison of CH_4 mole fraction with total air content at the same depths..

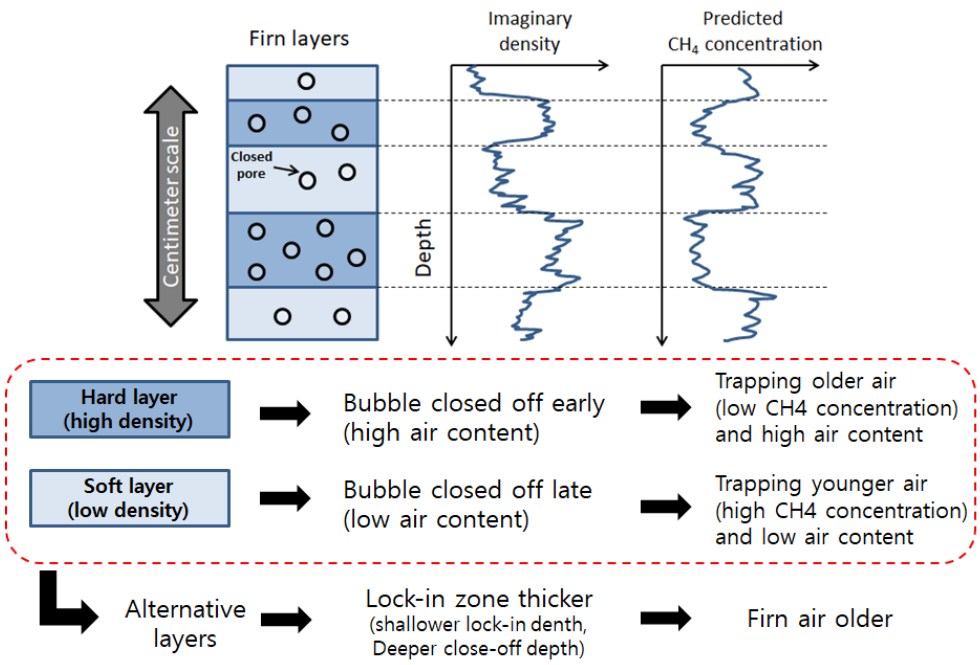

Figure A10. Concept cartoon of how different density layers affects the closed porosity and CH_4 mole fraction in the closed pores.